UNIVERSIDAD AUTONOMA DE MADRID

Grupo de Astrofísica
Universidad Autónoma de Madrid

Cosmic elemental abundances. Data sources

Stellar abundances

Abundance determination methods: Stellar abundances

- Abundance determinations from stars come from measurements of absorption lines
- Translation of absorption line strengths into abundances require application of stellar atmosphere models
- For most main sequence stars, plane-parallel, LTE models are enough, but
  - For stars with extended envelopes (giant and supergiants) spherical geometry is needed
  - For hot stars NLTE models are needed
- In any case, models should be line-blanketed

Emission and absorption of radiation

- Let us consider a light beam through a gas cloud $I_\nu(0) = 0$
- Two limiting cases arise:
  1. Optically thin medium
  2. Optically thick medium
- The equation of transfer is:

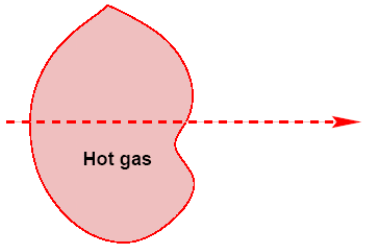

$$I_\nu(\tau_\nu) = I_\nu(0)e^{-\tau_\nu} + S_\nu(1 - e^{-\tau_\nu})$$

The optically thin case

- Optically thin medium

$$\tau_\nu \ll 1 \longrightarrow e^{-\tau_\nu} \simeq 1 - \tau_\nu$$

$$I_\nu(\tau_\nu) = S_\nu(1 - 1 + \tau_\nu) = \tau_\nu S_\nu$$

- If the gas is in LTE $\longrightarrow$ $I_\nu = \tau_\nu B_\nu \propto \alpha_\nu B_\nu$
- For a hot gas, the absorption coefficient is high at the frequencies of spectral lines

Optically thin medium

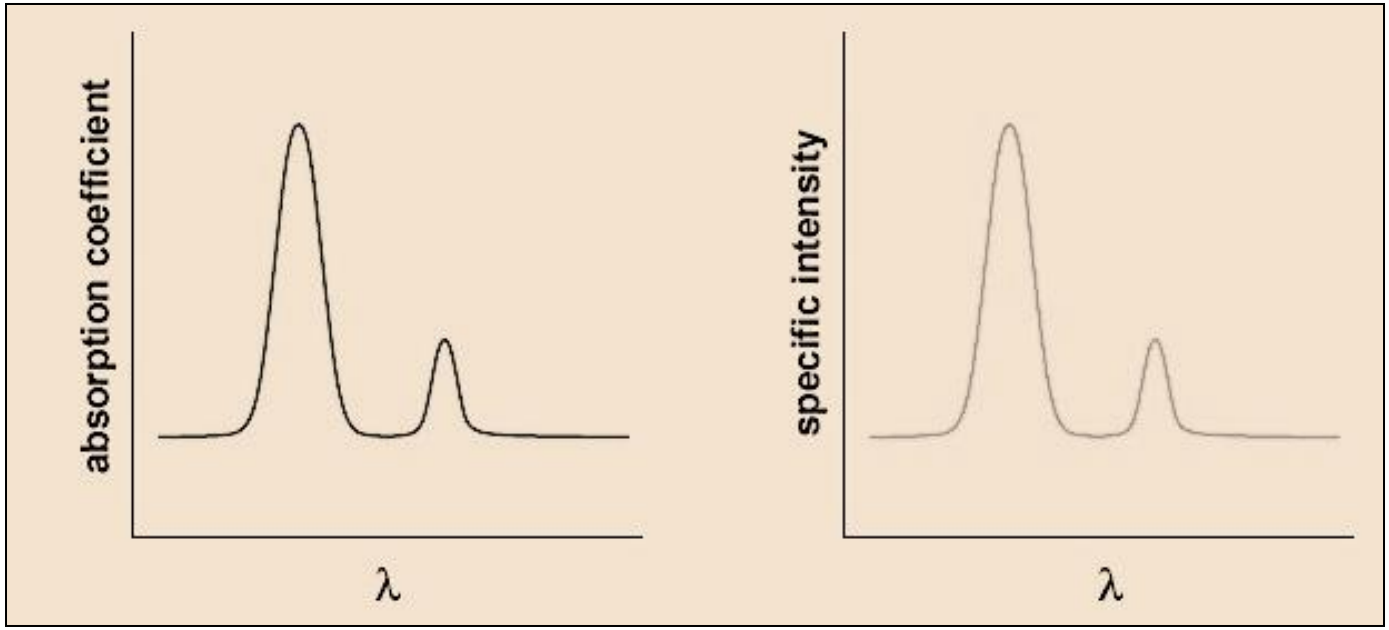

For an optically thin gas, we expect to get a spectrum with strong emission lines at the frequencies at which α_ν is large.

Emission line from an optically thin gas

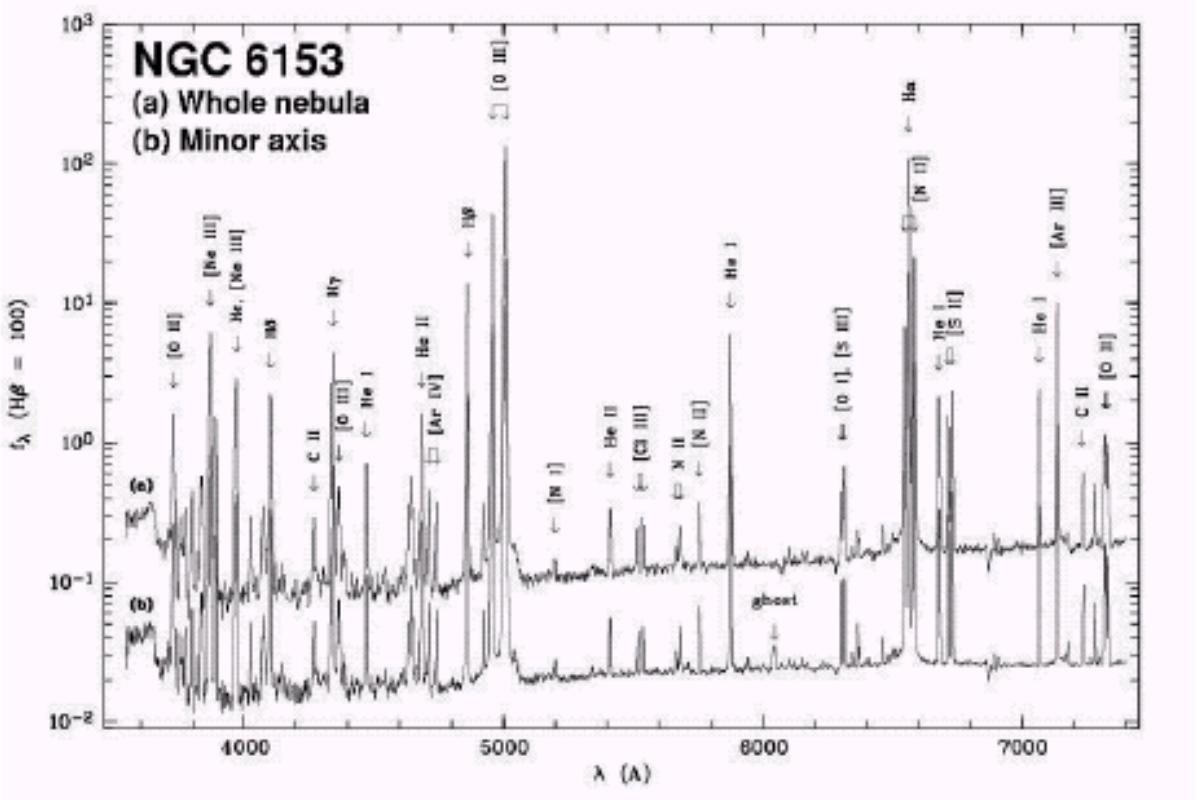

Emission lines produced in an optically thin gas volume with no illumination source in the background.

The optically thick case

- For an optically thick medium $\tau_\nu \gg 1$

$S_\nu(1 - e^{-\tau_\nu}) \rightarrow S_\nu$ and, in LTE, $I_\nu = S_\nu = B_\nu$

and the gas radiates as a black body.

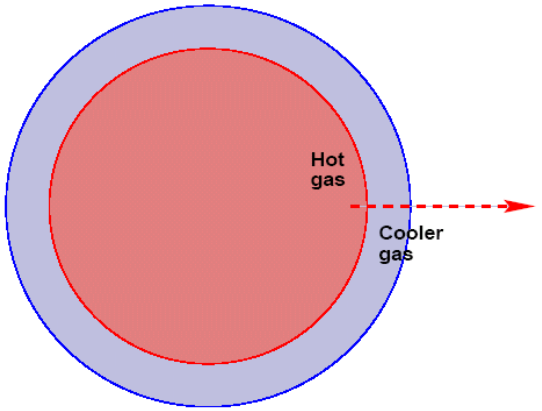

The interior of a star, such as the Sun, is optically thick and produces a continuum spectrum, although with absorption lines, since the source function S_ν varies through the stellar interior.

Emission and absorption agaisnt a continuum background

If $\tau_\nu \ll 1$

$$\begin{aligned} I_\nu(\tau_\nu) &= I_\nu(0)e^{-\tau_\nu} + S_\nu(1 - e^{-\tau_\nu}) \\ &= I_\nu(0)(1 - \tau_\nu) + \tau_\nu S_\nu \\ &= I_\nu(0) + \tau_\nu[S_\nu - I_\nu(0)] \end{aligned}$$

Again, we have two cases :

$S_\nu > I_\nu(0)$

The emergent intensity is larger at frequencies at which τ_ν is large $\rightarrow$ emission lines on top of a continuum background.

$S_\nu < I_\nu(0)$

The emergent spectrum is reduced at frequencies at which τ_ν is high $\rightarrow$ absorption lines on top of a continuum background.

An optically thin gas illuminated by radiation whose intensity is higher than the source function, produces an absorption. That would be the case for a cold gas in the line of sight to a very bright background object.

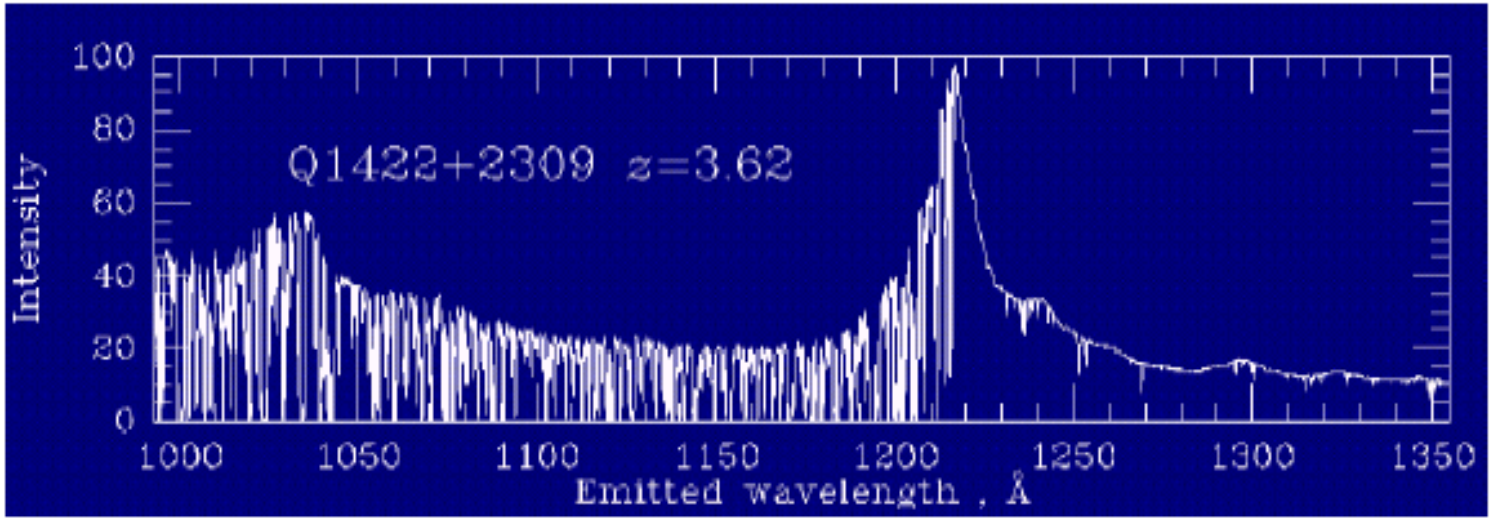

Absorption lines produced by neutral gas clouds in the line of sight bteeween the observer and a bright quasar.

Apsorption and emission in the solar spectrum

For an optically thick gas in LTE, $S_\nu(T) = B_\nu(T)$ that increases as T increases.

If $dT/dr < 0 \rightarrow S_\nu(T) < I_\nu(0)$. This is the case of the optical spectrum of the Sun.

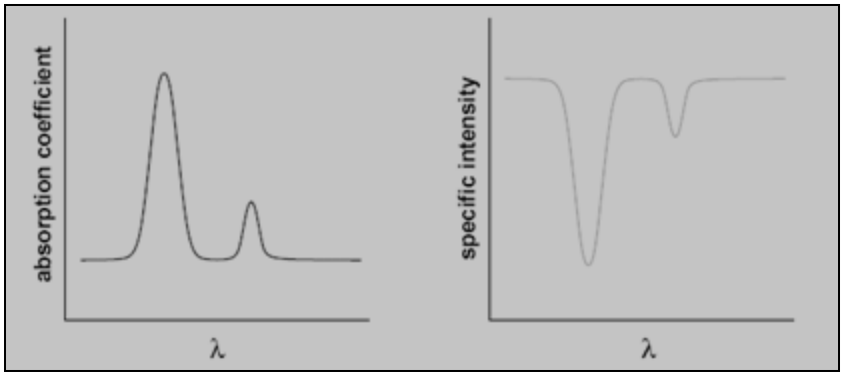

But in the UV, the radiation comes from regions where $dT/dr > 0$ (solar corona). In this case, $S_\nu(T) > I_\nu(0)$ and an emission spectrum on top of the continuum is observed.

Determinación de abundancias en estrellas

- The determination of stellar abundances is made through the analysis of absorption lines in high resolution spectra.

- This analysis can be made for stars in the Solar Neighbourhood and for brighest stars in clusters and in some galaxies of the Local Group.

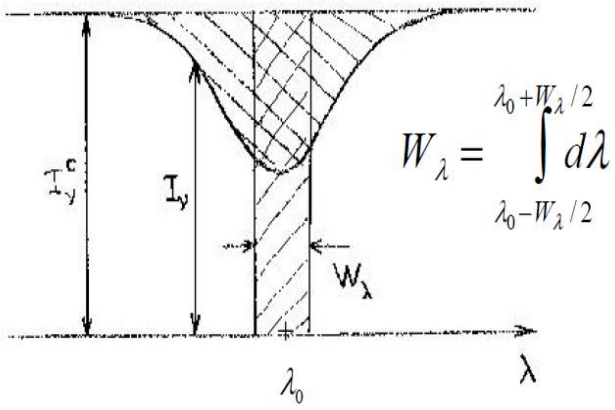

Spectral lines

- Spectral lines involve transitions between different energy states of ions, atoms or molecules.
- The opacity in the lines is due to different physical processes occurring in the stellar material, which determine the final absorption coefficient.
- The variation of this coefficient with wavelength configures the profile or shape of the line.

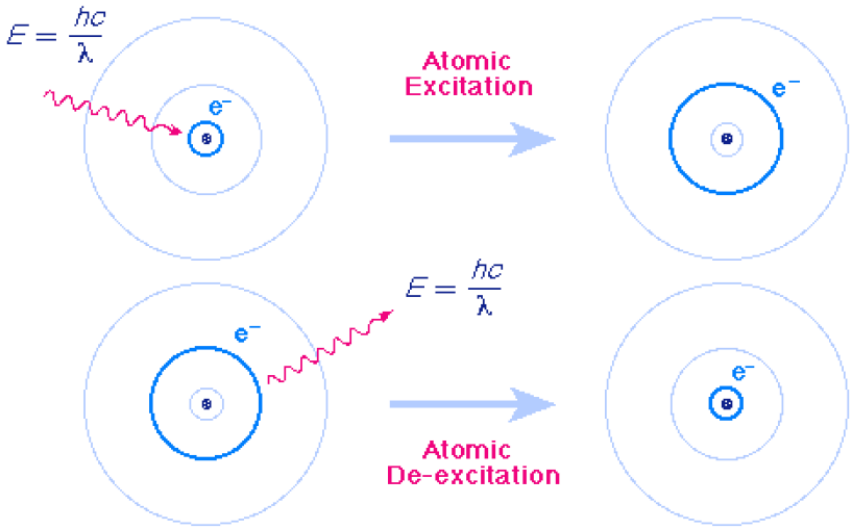

Absorption line profile

Line depth
(residual intensity)

$$R_l = \frac{F_c - F_l}{F_c} = 1 - \frac{F_l}{F_c}$$

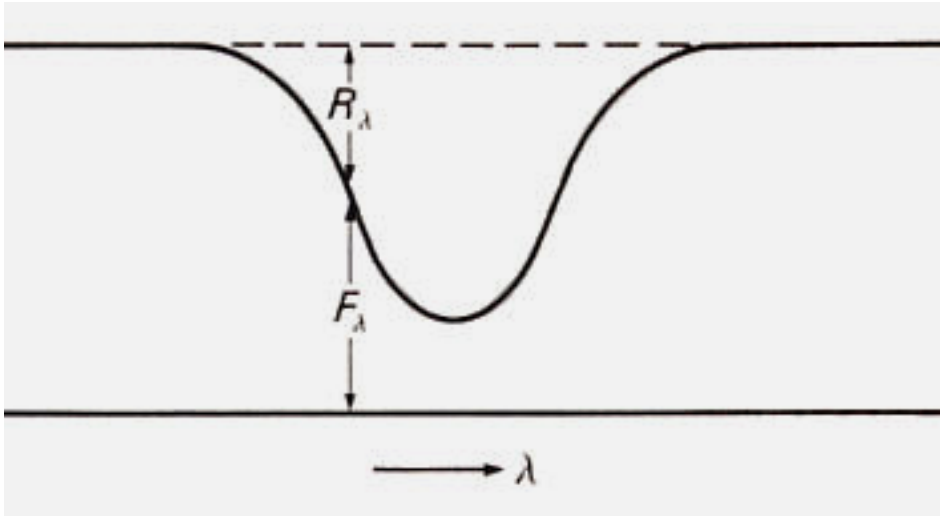

It's an adimensional quantity with values between 0 for a very weak line and 1 for a saturated line.

Line measurements

- **Line intensity**

$$I_l = \int_{\lambda_1}^{\lambda_2} \left(F_c - F_l \right) d\lambda$$

- **Equivalent width**
  - Defined as the width of a rectangle of height F_c and an area equal to the line intensity

$$W_l = \frac{I_l}{F_c} = \frac{1}{F_c} \int_{\lambda_1}^{\lambda_2} \left(F_c - F_l \right) d\lambda$$

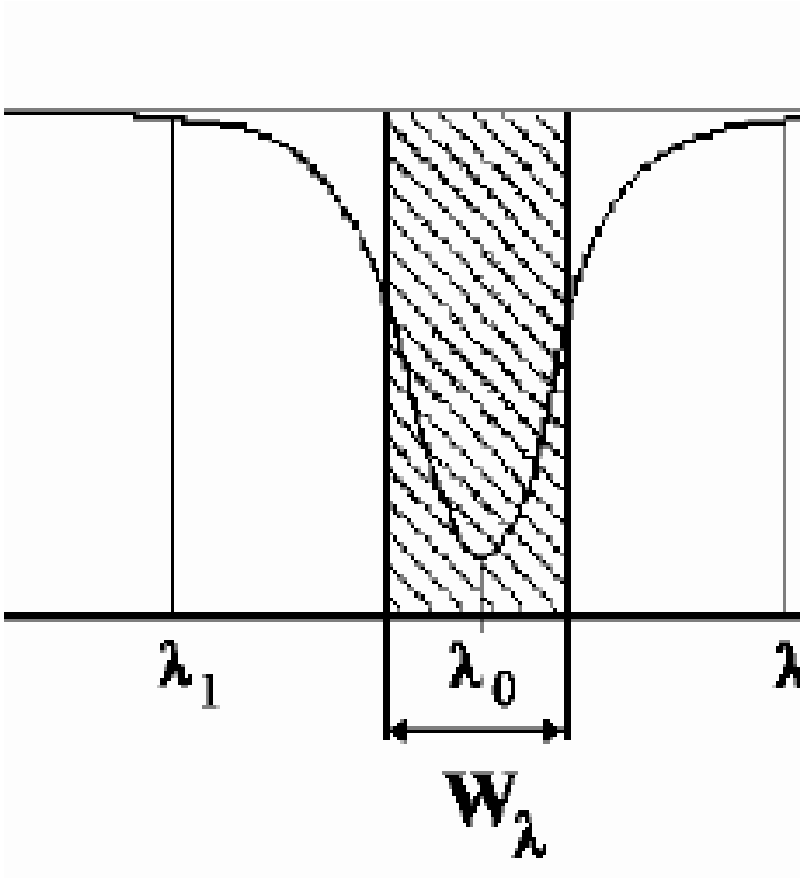

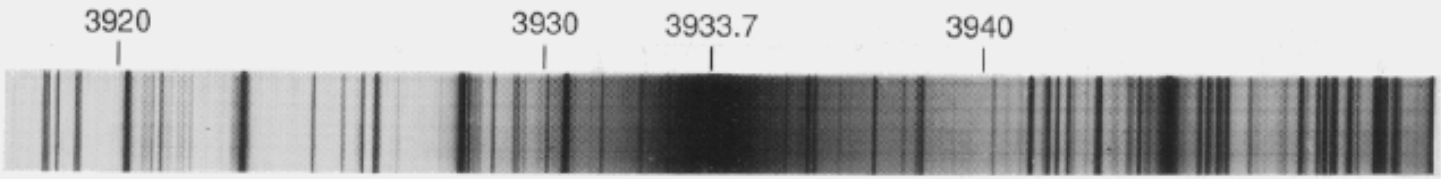

The continuum determination might be somewhat difficult

The profile of the **'K' line of Ca II** in the solar spectrum. The *H* and *K* lines of ionized calcium are the strongest lines recorded in the solar spectrum as observed from the surface of the earth. The wings are due to natural broadening and collisional broadening. The wavelength scale is given at the top of the figure.

Line formation: the classical view

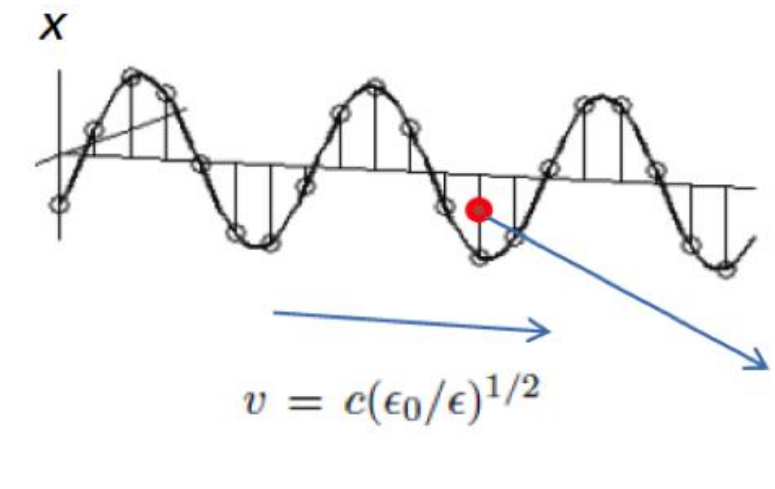

- Photons are sinusoidal variations of electro-magnetic fields
- When a photon passes by an electron in an atom, the changing fields cause the electron to oscillate
- Treat the electron as a classical harmonic oscillator:

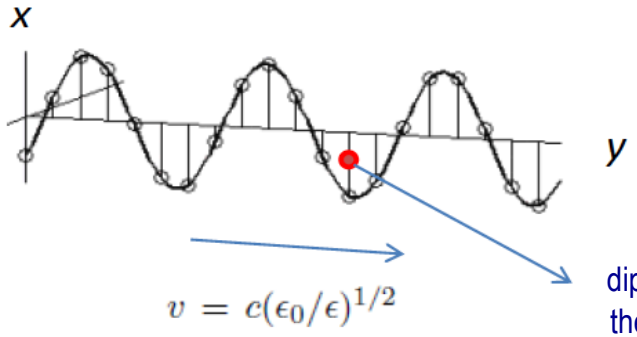

dipole oscillating in the x direction as a response to the electric field E

angular frequency of the wave

$$E = E_0 \exp\{i\omega[t - (\epsilon/\epsilon_0)^{1/2} y/c]\}$$

If N is the dipole density (each with an only electron) :

$$\frac{\epsilon}{\epsilon_0} = 1 + \frac{4\pi N e x}{E}$$

equation of motion :

$$\frac{d^2x}{dt^2} + \gamma\frac{dx}{dt} + \omega_0^2 x = \frac{e}{m}E_0 e^{i\omega t}$$

general solution :

$$x = x_0 \exp(i\omega t)$$

$$\longrightarrow \quad -\omega^2 x + i\gamma\omega x + \omega_0^2 x = \frac{e}{m}E_0 e^{i\omega t}$$

resonance frequency corresponding to the espectral line wavelength

$$\longrightarrow \quad x = \frac{e}{m}\frac{E}{\omega_0^2 - \omega^2 + i\gamma\omega}$$

Atomic absorption coefficient

- Classically, the absorption coefficient is given by:

$$\begin{aligned}\alpha &= \frac{2\pi e^2}{mc}\frac{\gamma/2}{\Delta\omega^2+(\gamma/2)^2}\\ &= \frac{e^2}{mc}\frac{\gamma/4\pi}{\Delta\nu^2+(\gamma/4\pi)^2}\\ &= \frac{e^2}{mc}\frac{\lambda^2}{c}\frac{\gamma\lambda^2/4\pi c}{\Delta\lambda^2+(\gamma\lambda^2/4\pi c)^2}\end{aligned}$$

and integrating for all frequencies :

$$\int_0^\infty \alpha d\nu = \int_{-\infty}^\infty \alpha d\Delta\nu = \frac{\pi e^2}{mc}$$

Classical damping constant

- γ is the **classical damping constant** and, for a classical harmonic oscillator, the shape of the spectral line depends on its size
- For $\nu - \nu_0 >> \gamma / 4\pi$, the line falls off as $(\nu - \nu_0)^{-2}$

Classical damping line profile

$$k_n r = \frac{N_0 e^2}{mc} \frac{g/4p}{(n - n_0)^2 + (g/4p)^2}$$

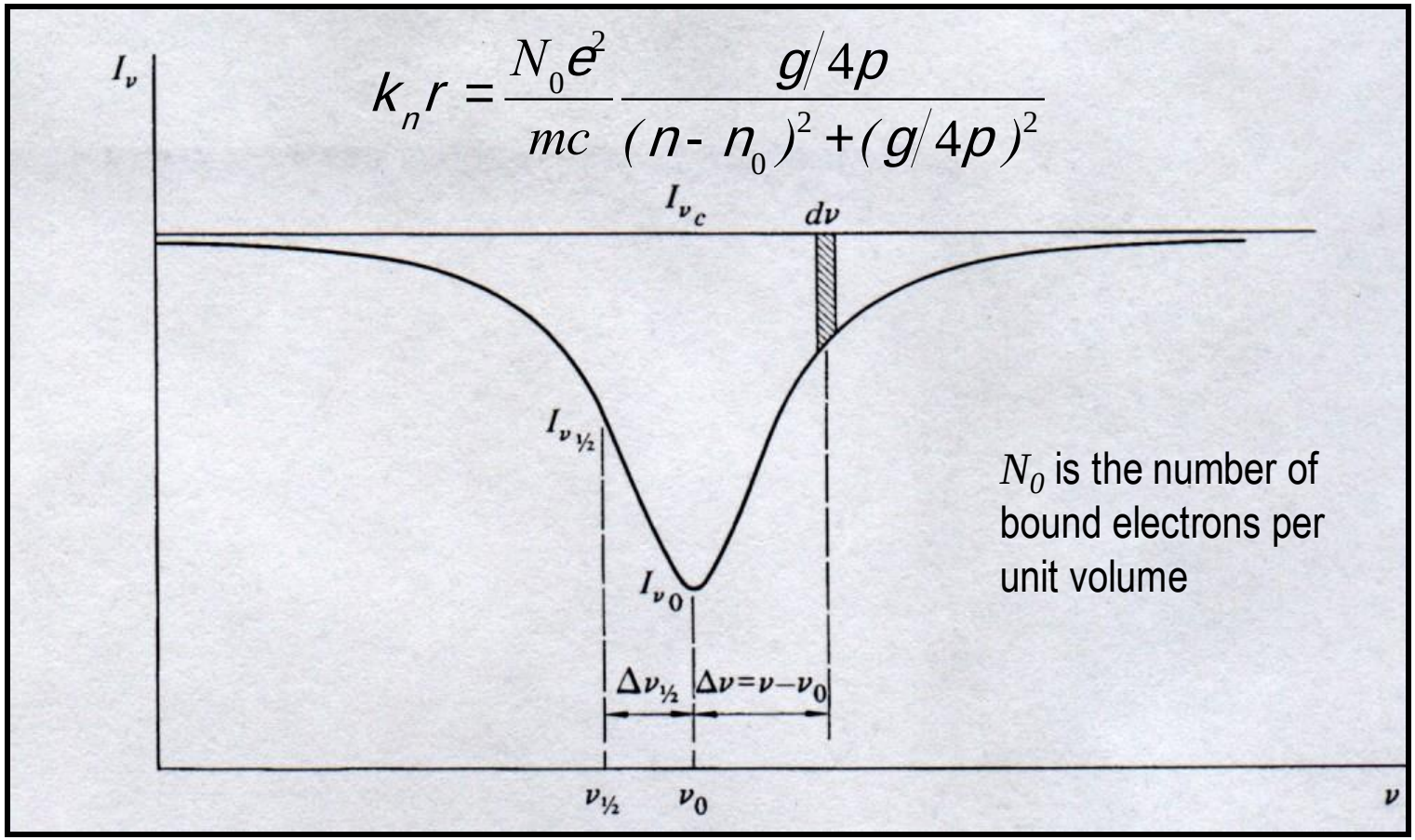

N_0 is the number of bound electrons per unit volume

Classical line profile

Look at a thin atmospheric layer between t_2 (the deeper layer) and t_1

$$I_\nu(\tau_2) = I_\nu(\tau_1)e^{-\kappa_\nu \rho \Delta x} \approx I_\nu(\tau_1)(1-\kappa_\nu \rho \Delta x)$$

$$I_\nu(\tau_2) - I_\nu(\tau_1) \approx \kappa_\nu \rho \Delta x I_\nu(\tau_1)$$

The line intensity at each frequency is proportional to κ_ν

At line center $\nu=\nu_0$, and $k_n r = \dfrac{4\pi e^2 N}{mc\gamma}$

Half the maximum depth occurs at $(\nu-\nu_0)=\gamma/4\pi$.

In terms of wavelength

$$\Delta\lambda_{1/2} = \frac{c}{n^2}\Delta\nu_{1/2} = \frac{c}{n^2}\frac{\gamma}{4\pi} = \frac{2\pi e^2}{3mc^2} = 0.000118 \text{ ang}$$

Very small – and the same for ALL lines!

Quantum correction: natural broadening

- Heisenberg's uncertainty principle: the electron in an excited state is only there for a short time, so its energy cannot have a precise value.
- Since energy levels are "fuzzy", atoms can absorb photons with slightly different energy, with the probability of absorption declining as the difference in the photon's energy from the "true" energy of the transition increases.
- The FWHM of natural broadening for a transition with an average waiting time of Δt_o is given by

$$(\Delta\lambda_{1/2}) = \frac{\lambda^2}{\pi c}\frac{1}{\Delta t_o}$$

- A typical value of $(\Delta\lambda)_{1/2} = 2 \times 10^{-4}$ Å. Natural broadening is usually very small.
- The profile of a naturally broadened linen is given by a **dispersion profile** (also called a damping profile) which has a Lorentzianf unctional form:

where γ is the "damping constant."

$$I_\nu \propto \frac{\gamma}{(\nu - \nu_0)^2 + \gamma^2}$$

Quantum corrections: the line profile

- Broadening depends on the lifetime of the level
- Levels with long lifetimes are sharp
- Levels with short lifetimes are fuzzy
- QM damping constants for resonance lines may be close to the classical damping constant
- QM damping constants for other Fraunhofer lines may be 5,10, or even 50 times bigger than the classical damping constant

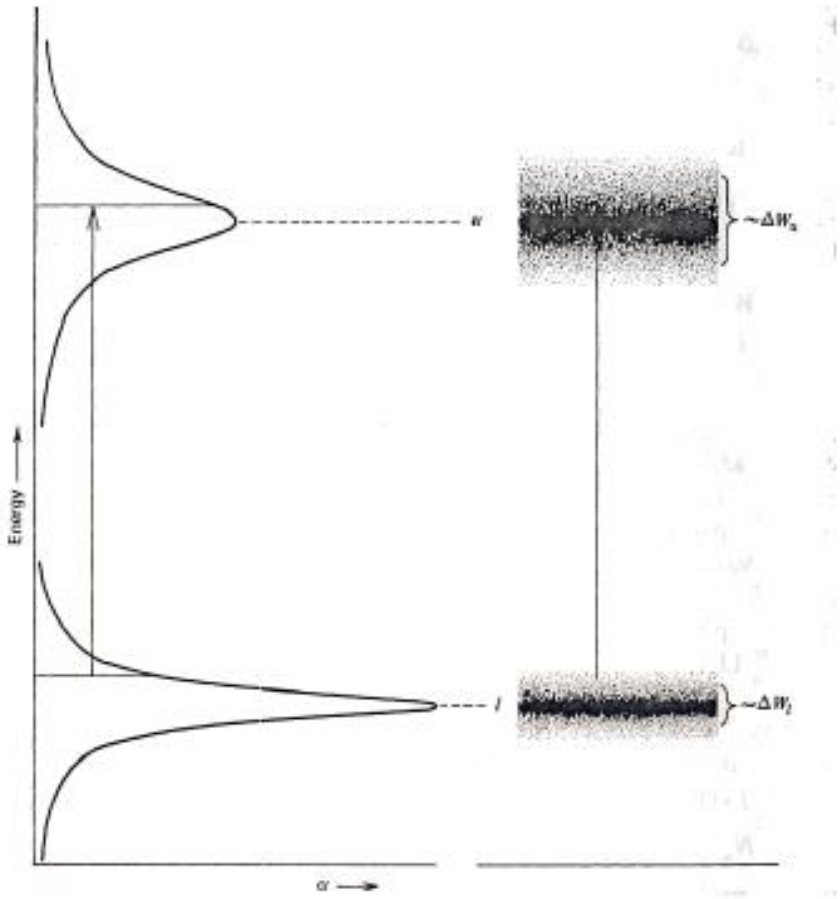

Quantum corrections: the oscillator strength

- We must relate the quantum damping constant to the lifetimes of the levels, or the probabilities of a given transition to take place. We can do so by …
- defining **the oscillator strength**, f, such as:

$$\int_0^\infty \alpha d\nu = \frac{\pi e^2}{mc} f$$

- f is related to the atomic transition probability B_{ul}:

$$\int_0^{\infty} a\, d\nu = h\nu B_{lu}$$

$$f = \frac{mc}{\pi e^2} h\nu B_{ul} = 7.5x10^{-7} \frac{B_{lu}}{l} = \frac{mc^3}{2\pi e^2 \nu^2} \frac{g_u}{g_l} A_{ul} = 1.9x10^{-15} l^2 \frac{g_u}{g_l} A_{ul}$$

Other broadening mechanisms

Broadening mechanisms contributing to the line profile

- Thermal broadening
- Collisional broadening
- Velocity fields:
  - macroturbulence
  - microturbulence

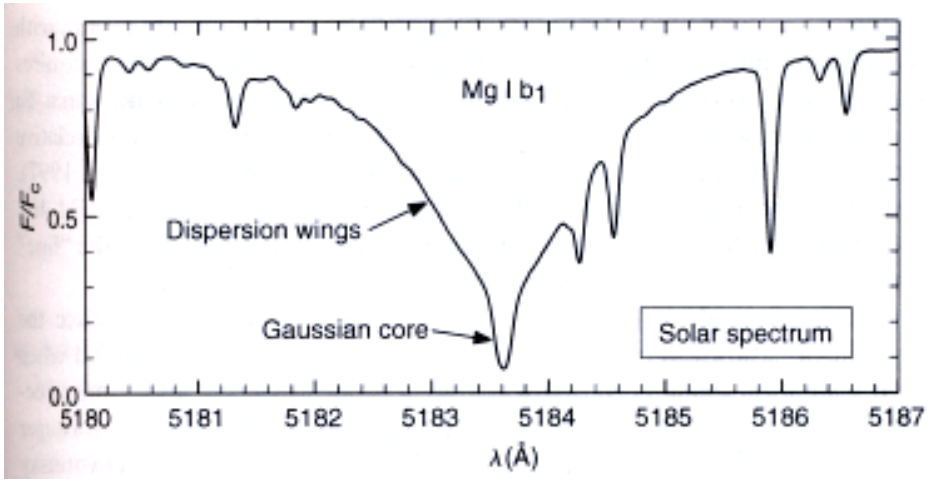

Thermal broadening

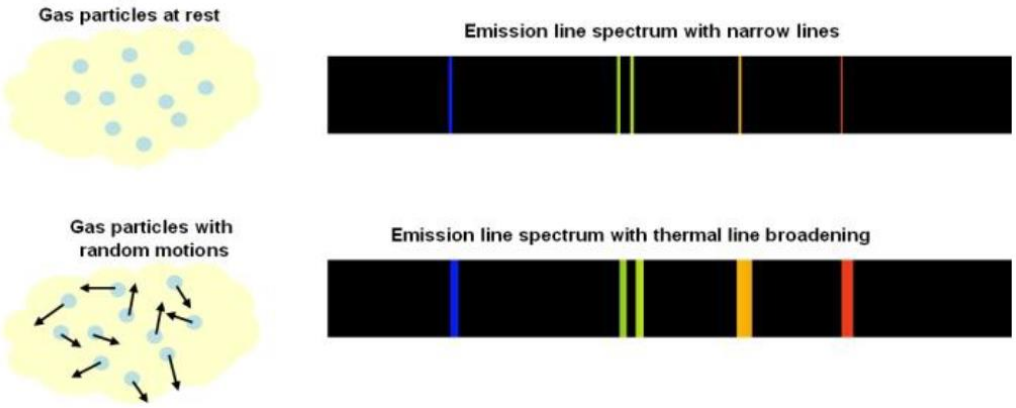

Due to the thermal motion, the atoms in the gas have a given velocity whose radial produces a Doppler displacement:

$$\frac{\Delta\lambda}{\lambda} = \frac{\Delta\nu}{\nu} = \frac{v_r}{c}$$

The distribution of $\Delta\lambda\ (\propto v_r)$ yields the line profile.

Thermal broadening

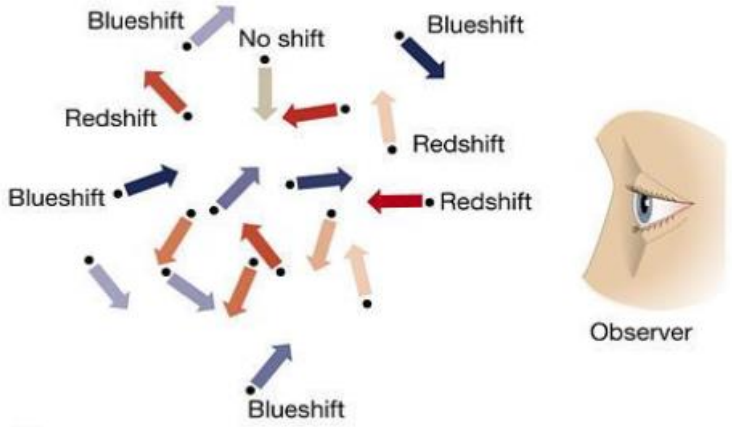

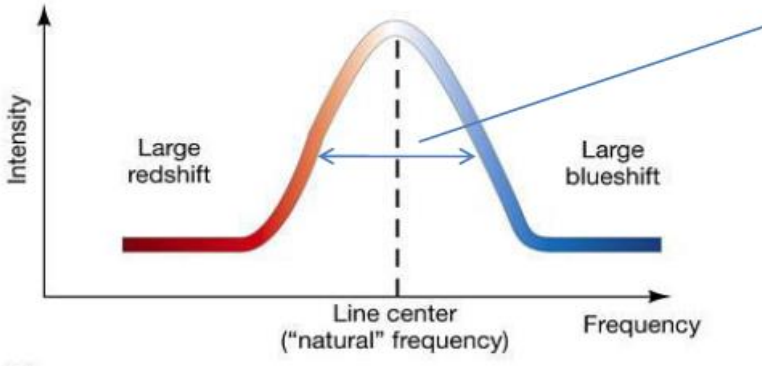

This line broadening is proportional to $\Delta\lambda_0$

Thermal broadening

- Thermal broadening is controlled by the thermal (Maxwellian) velocity distribution:

$$\frac{dN(v_r)}{N_{Total}} = \left(\frac{m}{2\pi kT}\right)^{2/3} e^{-\left(\frac{mv_r^2}{2kT}\right)} dv_r$$

where v_r is the line-of-sight velocity component

- The Doppler width associated with the velocity v_0 (where the variance $v_0^2 = 2kT/m$) is :

$$\Delta\lambda_D = \frac{v_0}{c}\lambda = \frac{\lambda}{c}\left(\frac{2kT}{m}\right)^{1/2} = 4.3x10^{-7}\,\lambda(T/\mu)^{1/2}$$

and λ is the wavelength of line center and μ is the mean molecular weight.

Collisional broadening

Due to the presence of other ions in the vicinity of the absorbent ion which perturb its energy levels.

$$\Delta E = \frac{const.}{R^n}$$

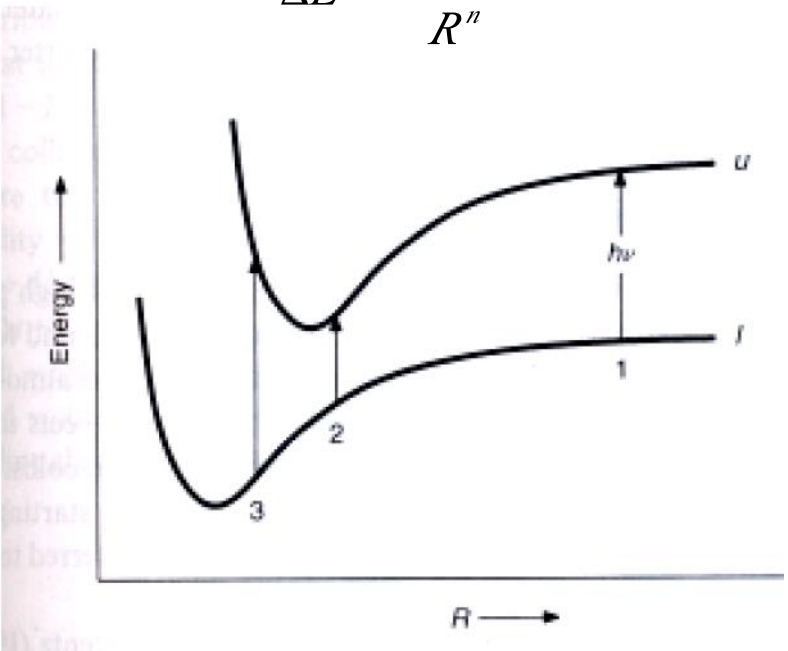

The effect depends of the perturber type:

- n=2 → p^+ or e^- over H (lineal Stark)
- n=4 →ions or e^- over other ions at high temperature (quadratic Stark)
- n=6 →H over other elements in cold stars (van der Waals)

Under the impact approximation

$$a = const. \frac{g/4p}{(n - n_0)^2 + (g_n/4p)^2}$$

Where $\gamma_n = 2/\Delta t_0$ is the average collision time and depends on the atmosphere depth.

Collisional broadening effects

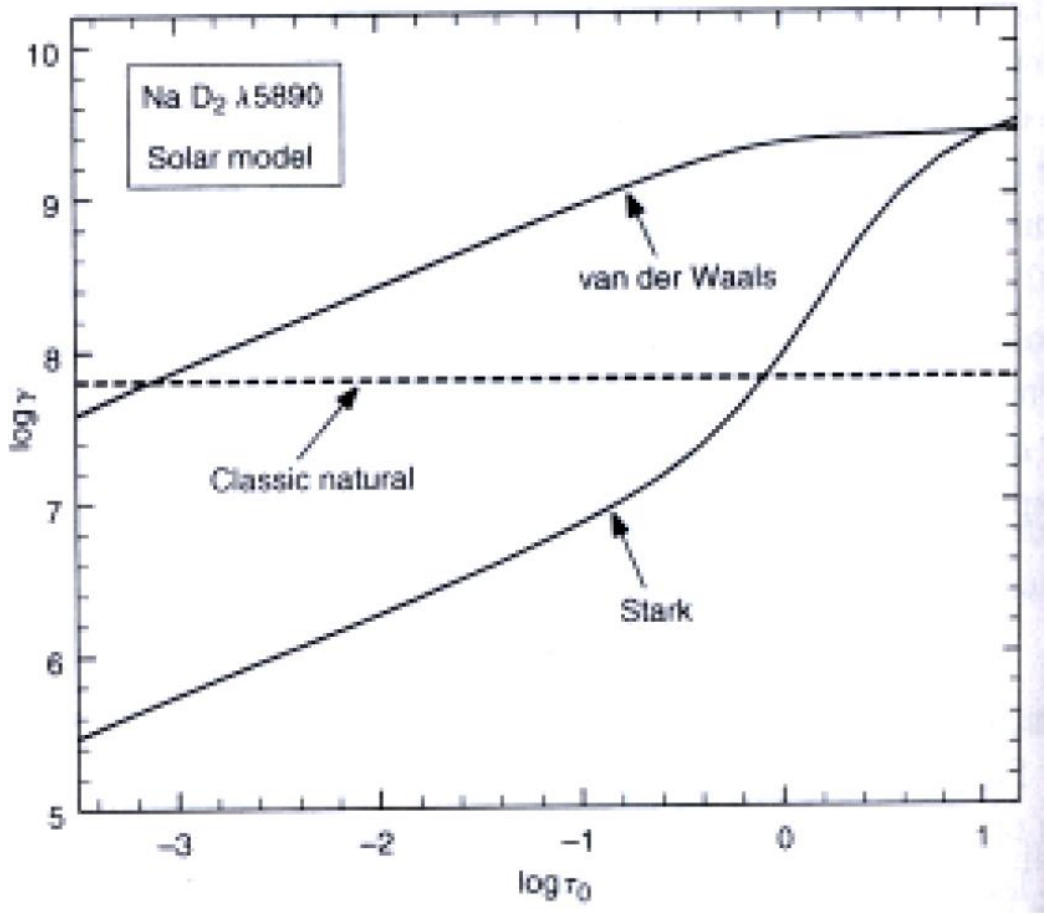

Velocity fields: convection

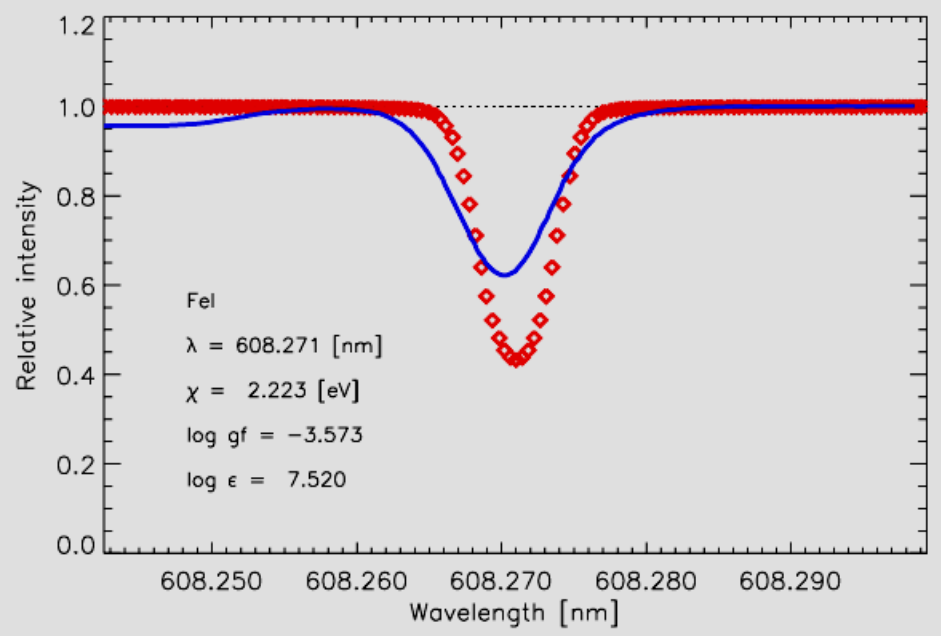

- **Macroturbulence** → motions at a scale larger than the photon mean free path.
- **Microturbulence** → motions at a scale smaller than the photon mean free path.
- Both add components to the Doppler broadening.
- Microturbulence, parametrized by v_{mac} and microturbulence, parametrized by v_{mic} .

Velocity fields: rotation

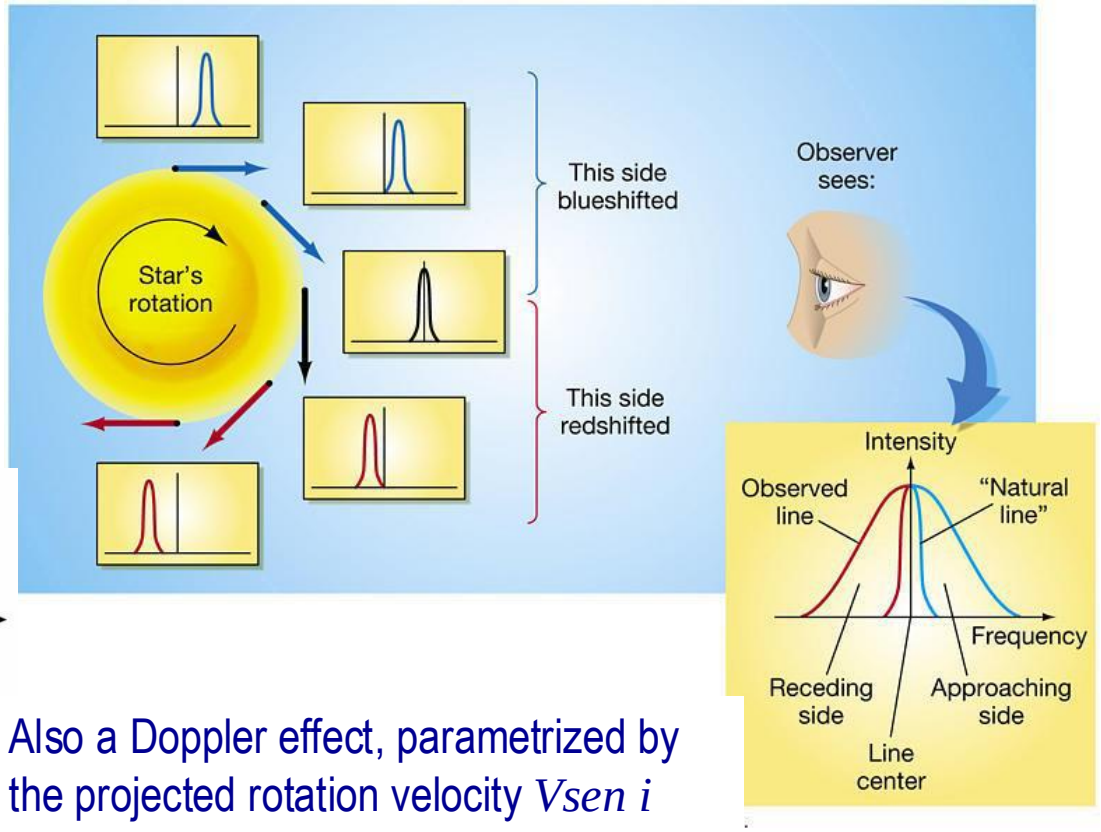

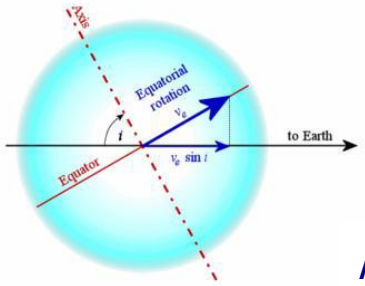

Also a Doppler effect, parametrized by the projected rotation velocity $Vsen\ i$

Rotational broadening examples

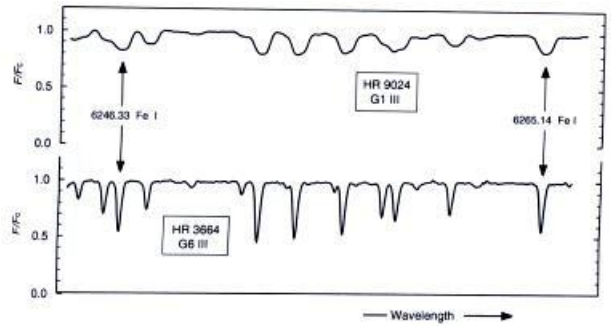

Fig. 18.7. These two G giants illustrate the Doppler broadening of the line profiles by rotation. HR 3664 shows low rotation, comparable to the macroturbulence broadening, of a few km/s, while HR 9024 shows rotational broadening that is substantially larger. Data taken at the Elginfield Observatory.

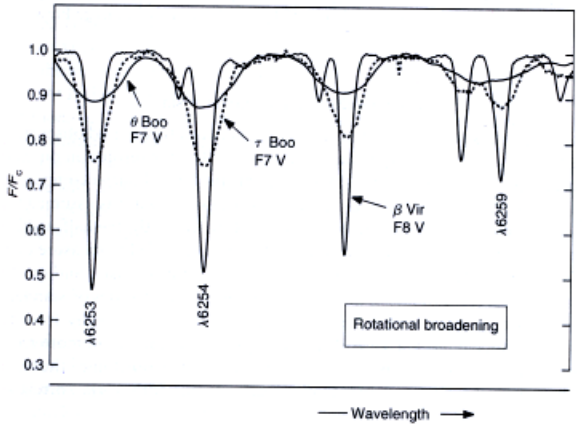

Fig. 18.8. The rotational broadening in three F dwarfs are compared. Data from the Elginfield Observatory.

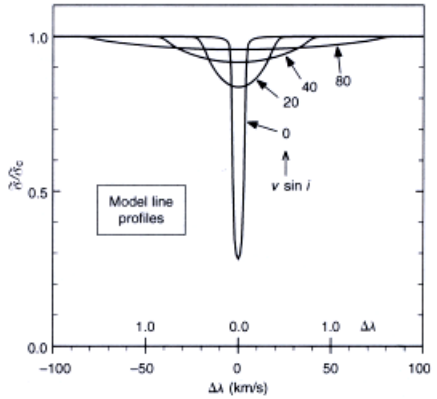

Fig. 18.6. Computed profiles illustrate the broadening effect of rotation. The profiles are labeled with $v \sin i$ in km/s. The equivalent width is conserved.

The total absorption coefficient and line profile

- Considering all types of broadening, the total absorption coefficient is:

$$\alpha = \alpha\,(\text{natural}) + \alpha\,(\text{Doppler}) + \alpha\,(\text{collisional})$$

normalised as $$\int_0^{\infty} a\,dn = \frac{pe^2 f}{mc}$$

- The natural and collisional broadening profiles are both of Lorentzian form, therefore we can use an only Lorentzian profile with

$$\gamma = \gamma_{\text{natural}} + \gamma_{\text{collisional}}$$

The total Doppler profile

- All velocity dependent broadening mechanisms: thermal, turbulence and rotation, combine in a total Gaussian profile where

$$(\Delta\lambda)_{1/2} = \frac{2\lambda}{c}\sqrt{\left(\frac{2kT}{m} + v^2_{non-th}\right)^2 ln\,2}$$

- Typical values for $(\Delta\lambda)_{1/2}$ are a few tenths of an angstrom. The line depth for Doppler broadening decreases exponentially from the line center.

The Voigt profile

- The convolution of a dispersion profile and a Gaussian profile is known as the **Voigt profile.**

$$V(\Delta\nu, \Delta\nu_D, \gamma) = \int_0^\infty \frac{\gamma/4\pi^2}{(\Delta\nu - \Delta\nu_1)^2 + (\gamma/4\pi)^2} \frac{1}{\pi^{1/2}\Delta\nu_D} e^{-\left(\frac{\Delta\nu}{\Delta\nu_D}\right)^2} d\nu_1$$

- In general, the shapes of spectra lines are defined in terms of Voigt profiles, which are tabulated for their use in computations
- The final form of the Voigt profile depends on a parameter α, namely the ratio of the damping width γ /2 to the Doppler width $\Delta\nu_D$: $\boldsymbol{\alpha = \gamma / (2 \cdot \Delta\nu_D)}$
- Voigt functions are dominated by Doppler broadening at small $\Delta\lambda$, and by radiation or collisional broadening at large $\Delta\lambda$
- For weak lines, it's the Doppler core that dominates
- In solar-type stars, collisions dominate γ, so one needs to know the damping constant and the pressure to compute the line absorption coefficient
- For strong lines, we need to know the damping parameters to interpret the line.

Profile comparison

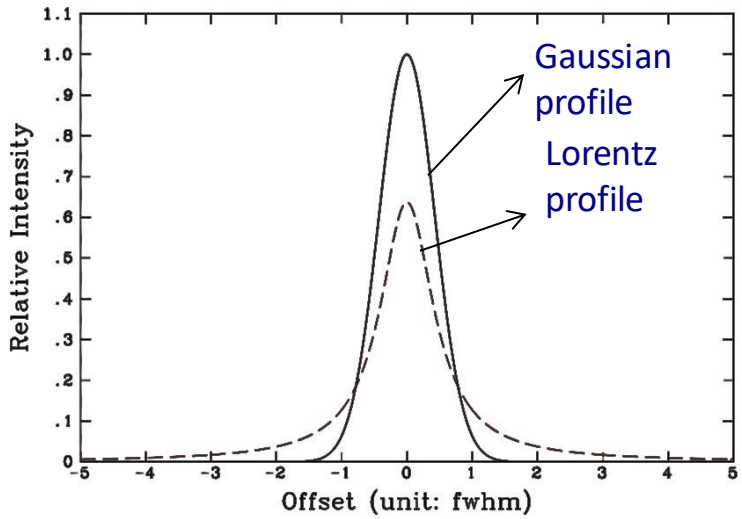

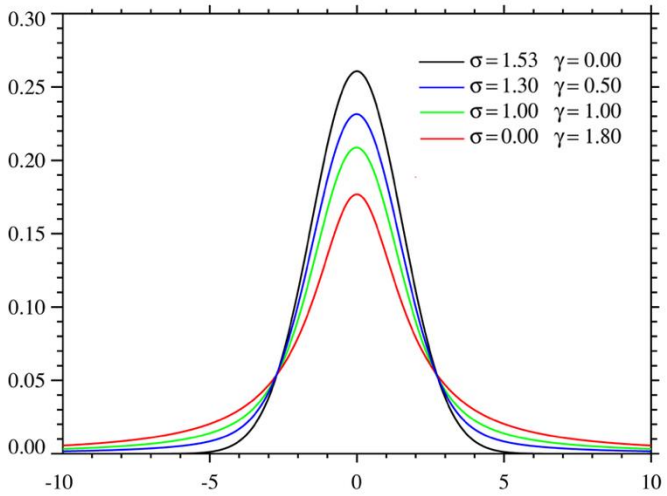

Shape of absorption lines

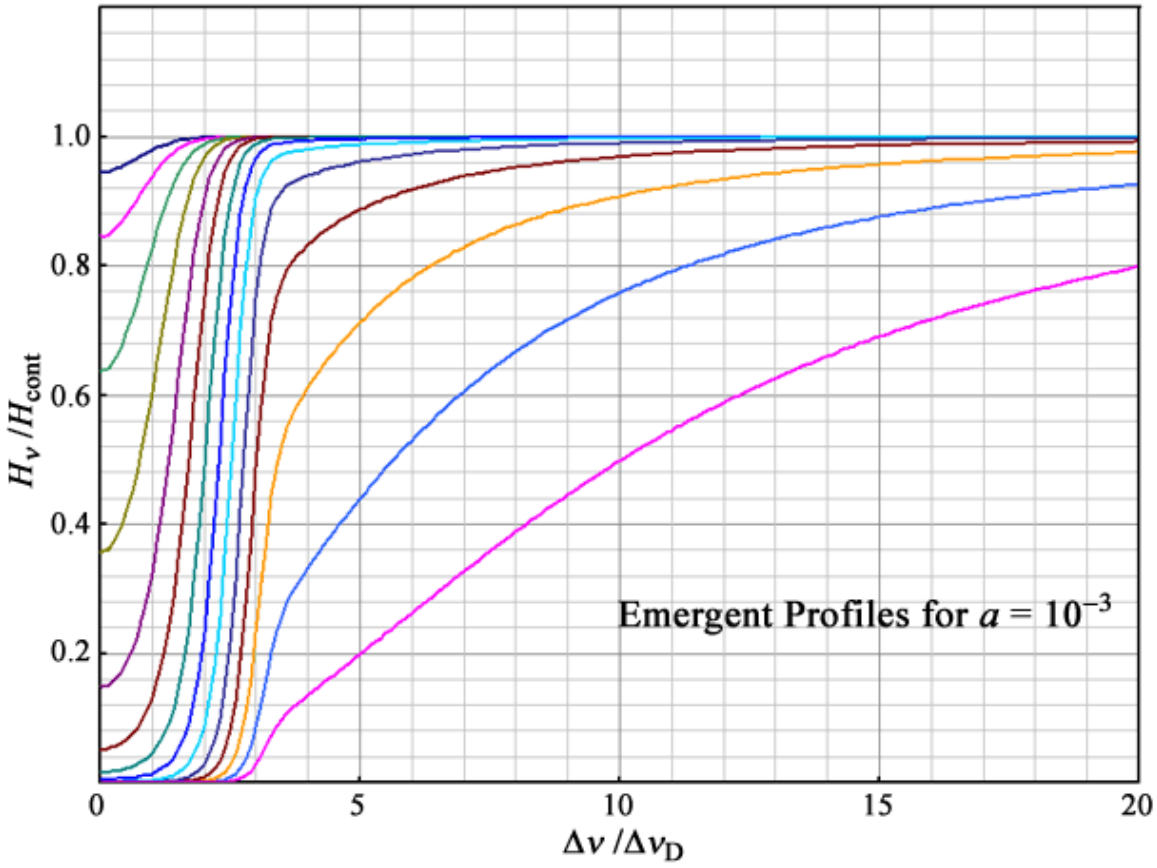

Observed line profile

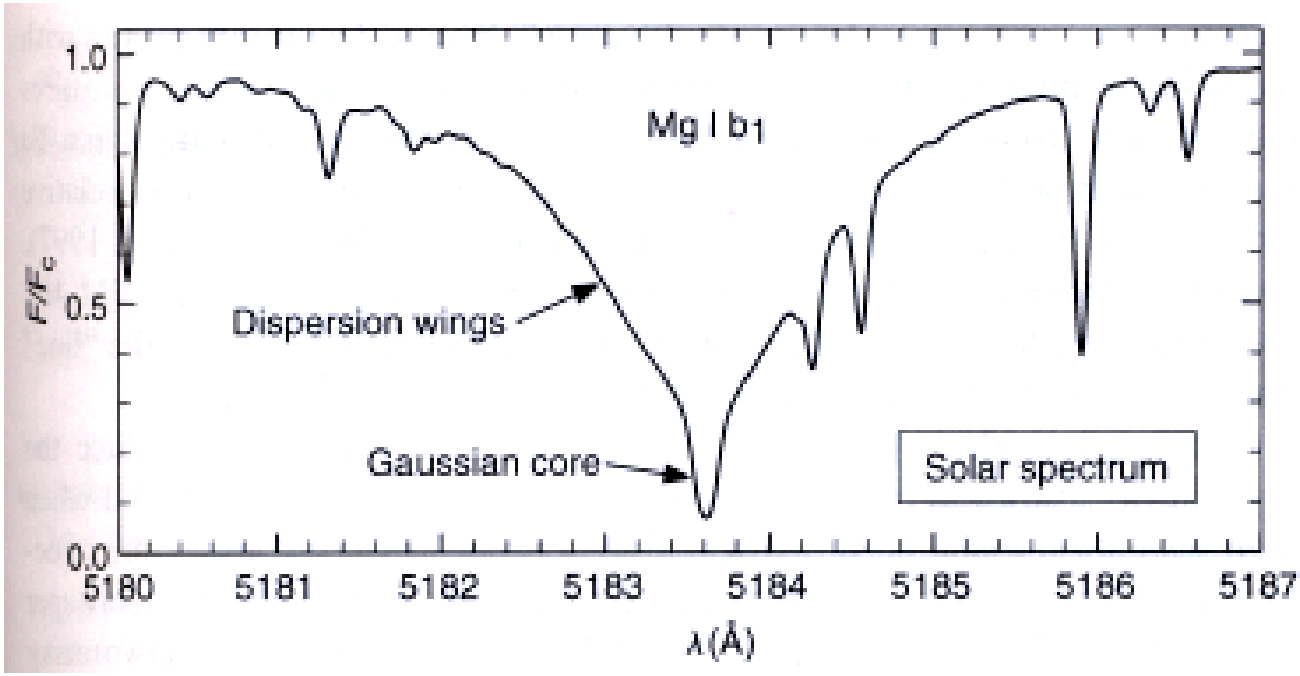

Line formation regions

- The different parts of a line are formed at different optical
- depths in the atmosphere of the star.

- The line core is formed in regions of lower optical depths, while the line wings are formed in regions of higher optical depths.
- In normal stars, temperature decreases outward in the atmosphere → line cores come from cooler regions than the wings.

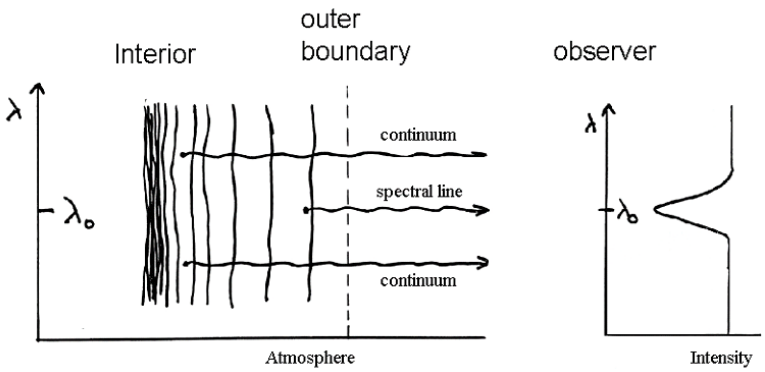

Line formation regions

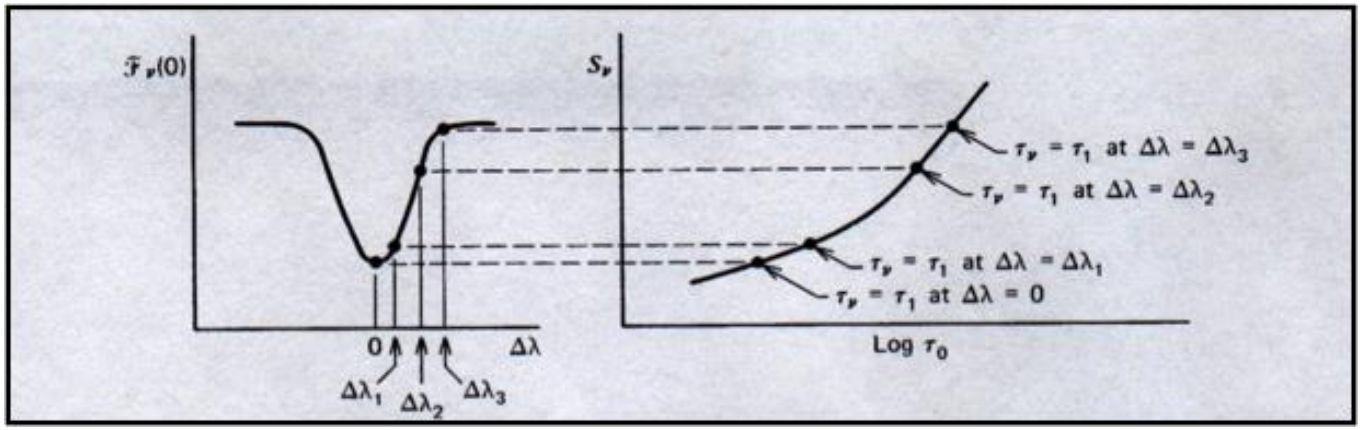

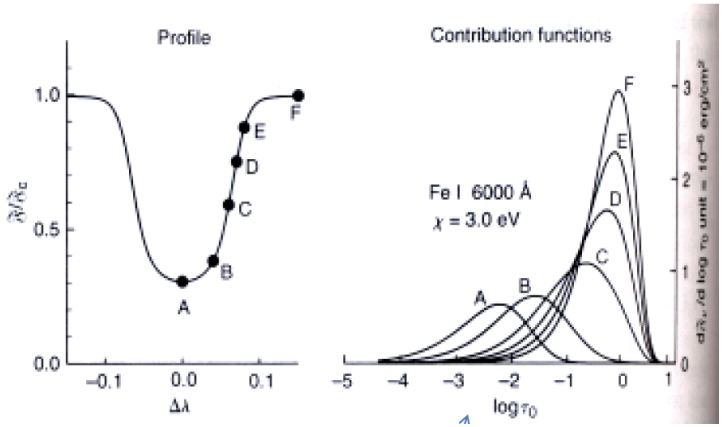

- **Line intensity**

$$I_l = \int_{l_1}^{l_2} \left(F_c - F_l \right) dl$$

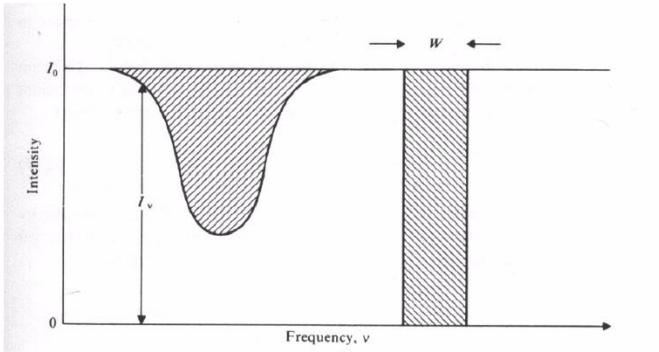

- **Equivalent width**
  - Defined as the width of a rectangle of height F_c and an area equal to the line intensity

$$W_l = \frac{I_l}{F_c} = \frac{1}{F_c} \int_{l_1}^{l_2} \left(F_c - F_l \right) dl$$

Equivalent width and optical depth

- The equivalent width is related to the optical depth in the line of sight.
- We can write $W_l = \frac{l_o^2}{c} \int_0^{\infty} \left(1 - \frac{I_n}{I_{n,c}}\right) d\nu$ and, since

$I_n = I_{n,c} e^{-\tau_n}$ we have $W_l = \frac{l_o^2}{c} \int_0^{\infty} \left(1 - e^{-\tau_n}\right) d\nu$

where we have made use of the relation $I_l dl = I_n d\nu$

Optical depth and number of absorbers

- The optical depth is related to the column density of absorbers along the line of sight (usually measured in cm^{-2})

- $$\tau_\nu = \int_0^D k_\nu ds = \int_0^D a_\nu n_i(s)$$

where k_ν is de volume opacity for transition $i \rightarrow j$, a_ν is the absorption cross section and n_i is the volume number density, so that τ is adimensional.

$$a_n(i,j) = \frac{c^2}{8\pi n^2}\frac{g_i}{g_j}A_{ij}f_n(s) = a_0 f_n(s)$$

Equivalent width and number of absorbers

$$A_{ij} = \frac{8\pi^2 e^2 \nu^2}{m_e c^3} \frac{g_i}{g_j} f_{ij} \quad \Rightarrow \quad a_\nu(i,j) = \frac{\pi e^2}{m_e c} f_{ij} \phi_\nu(s)$$

Now $$\tau_\nu = \frac{\pi e^2}{m_e c} f_{ij} \int_o^D \phi_\nu(s) n_i(s) ds$$ and if $\phi_\nu \neq \phi_{\nu(s)}$

$$\tau_\nu = \frac{\pi e^2}{m_e c} f_{ij} \phi_\nu N_i$$ that provides the relation between the equivalent width, W_λ, and the number of absorbers, N_i.

Chemical analysis: the curve of growth

- The equivalent width W_λ of a line is expected to depend on the number of atoms N in the atmosphere capable to absorb the transition involved, and hence on the temperature and density (or pressure) inside the gas, and **on the chemical composition of the star.**
- But also, the strength of a given line will depend on atomic properties, summarized by the f factor, assumed to be known.

- Then: $$W_l = W_l(N.f)$$

where N stands for the column density of the atoms producing the line

The curve of growth

- The curve of growth (CoG) provides the relation between the equivalent width of a line and the chemical abundance of the element producing it.

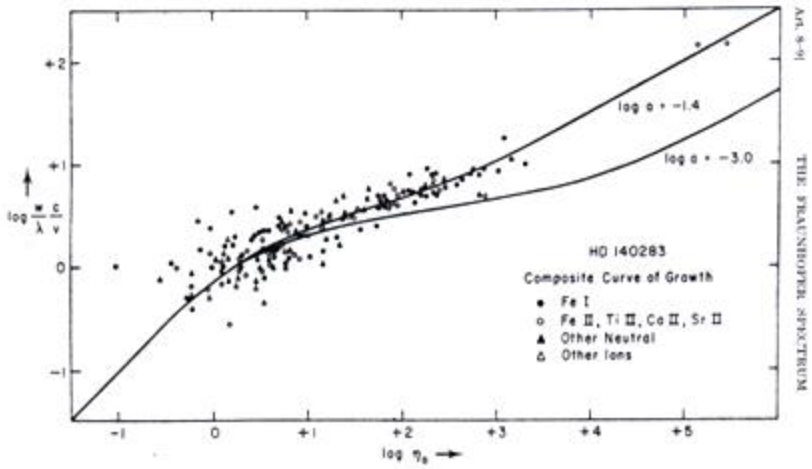

- τ_ν depends on the profile function, i.e., at a given frequency the optical depth can be greater or smaller, depending on ϕ_ν, for a given N.
- Then, the CoG is not linear and depends on the broadening mechanisms affecting the line.

Regions of the curve of growth

- As we saw above, $W_l = \frac{l_o^2}{c}\int_0^{\infty}\left(1- e^{-t_n}\right)d\nu$
- If τ <<1

$$\left(1- e^{-t_n}\right) \approx t_n \text{ and } W_l \approx \frac{l_0^2}{c}\int_0^{\infty} t_n d\nu$$

$$\frac{W_l}{l_0} = \frac{l_0}{c}\frac{\pi e^2}{m_e c} N_i f_{ij}\int_0^{\infty} f_n d\nu = \frac{\pi e^2}{m_e c^2} N_i l_0 f_{ij} \Rightarrow \text{straight line}$$

- This is called the linear part of the CoG. This linear relation is **independent of the line profile.**

Curve of growth: lineal part

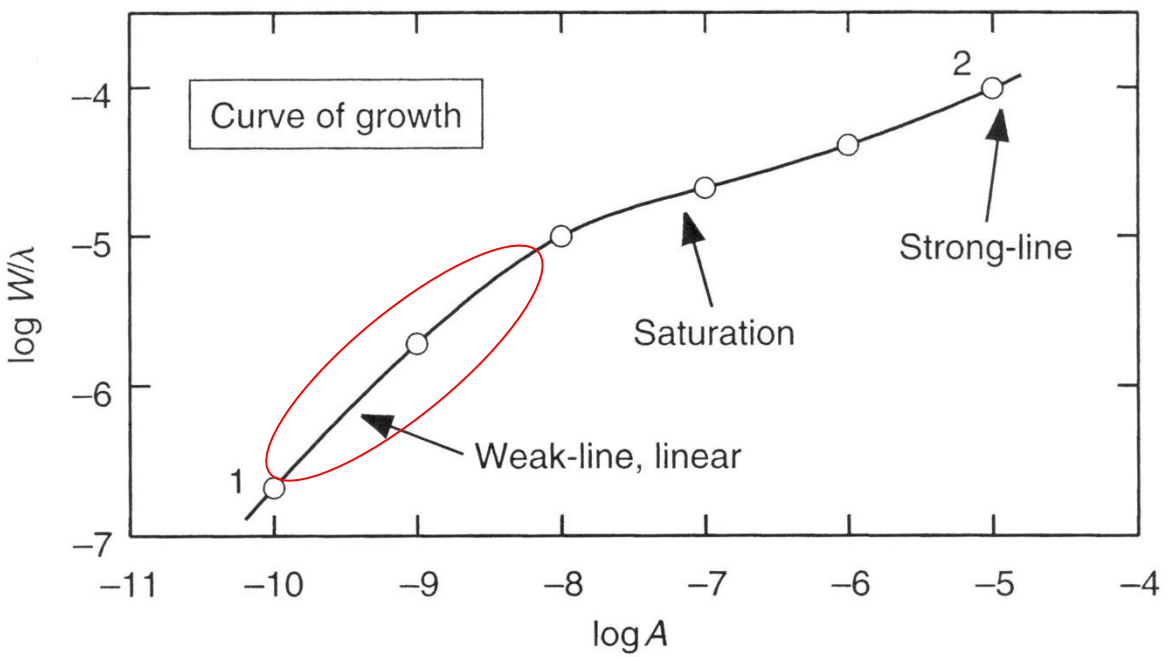

Curve of growth: saturated part

- As the line strength increases, a progressive increase in N produces no significant change in W_λ. It is said that **the line is saturated** and looks as a *plateau* in the curve of growth.

- The previous integral has to be calculated numerically and some approaches can be made to show that

$$W_l \mu \left(ln\, t_0 \right)^{1/2}$$

Curve of growth: saturated part

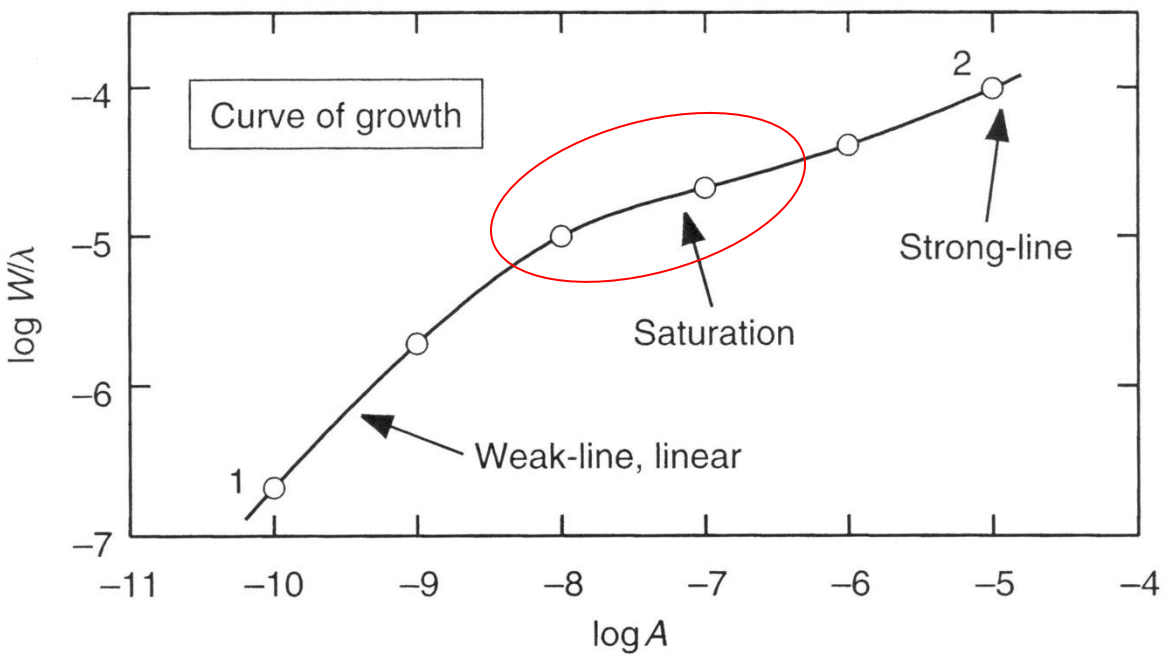

Curve of growth: square root part

- Finally, for very strong lines, the Gaussian core is saturated and the Lorentzian damping wings dominate.

- In that case, it can be shown that

$$W_\lambda \propto \left(\lambda_0^2 N_i \right)^{1/2}$$

- This is called the **square-root part** of the curve of growth

Curve of growth: square root part

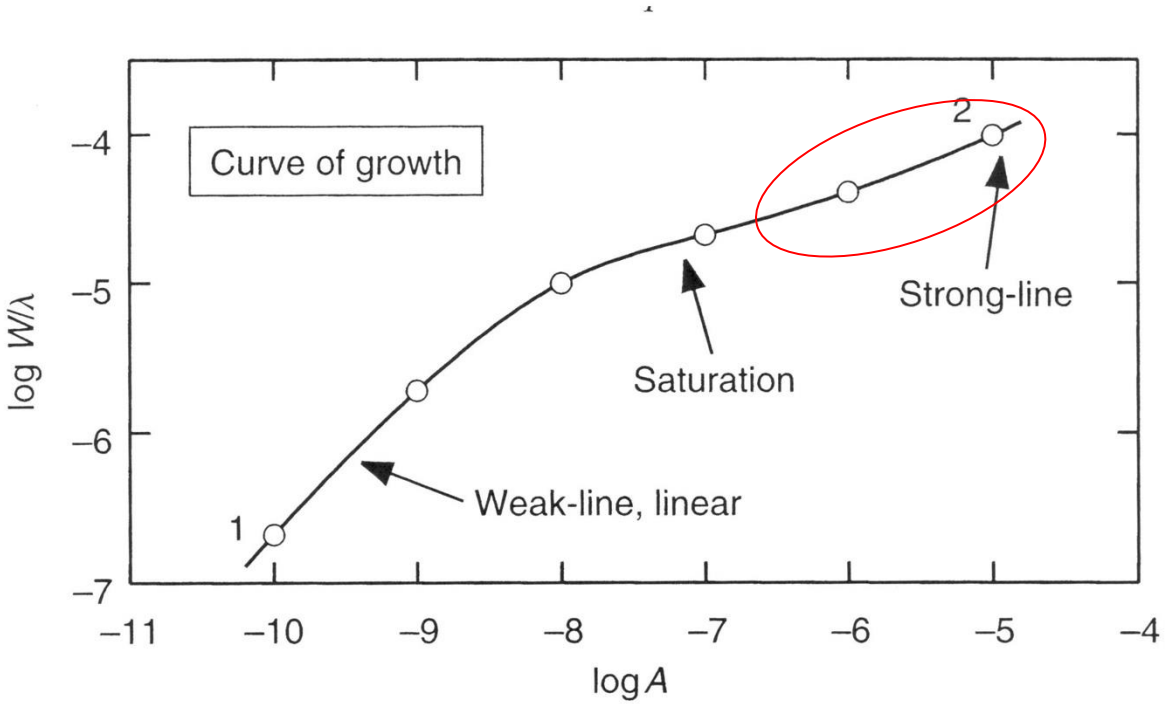

Curve of growth and line shape

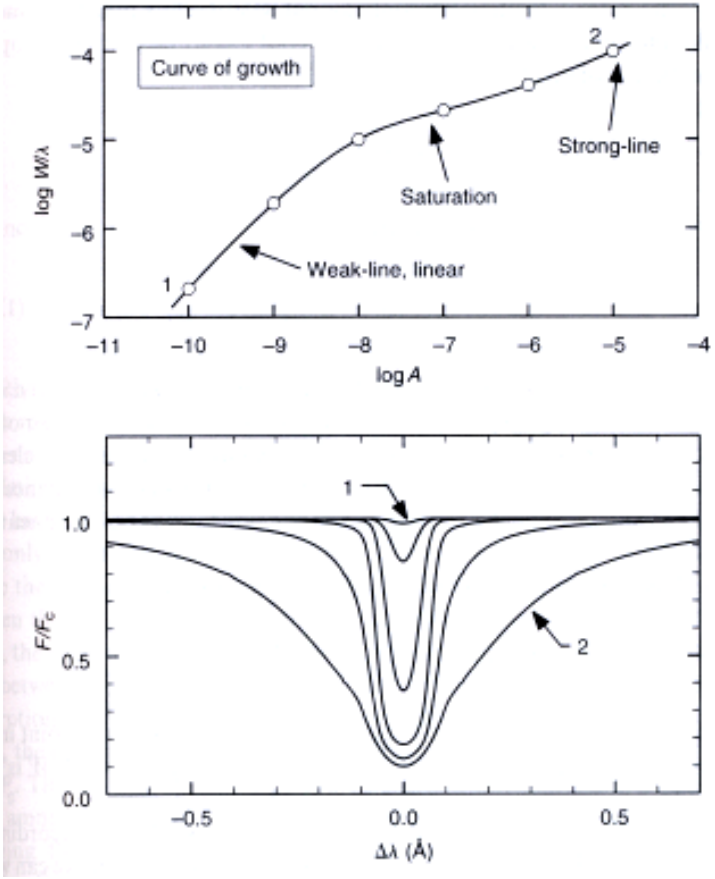

Empirical curves of growth

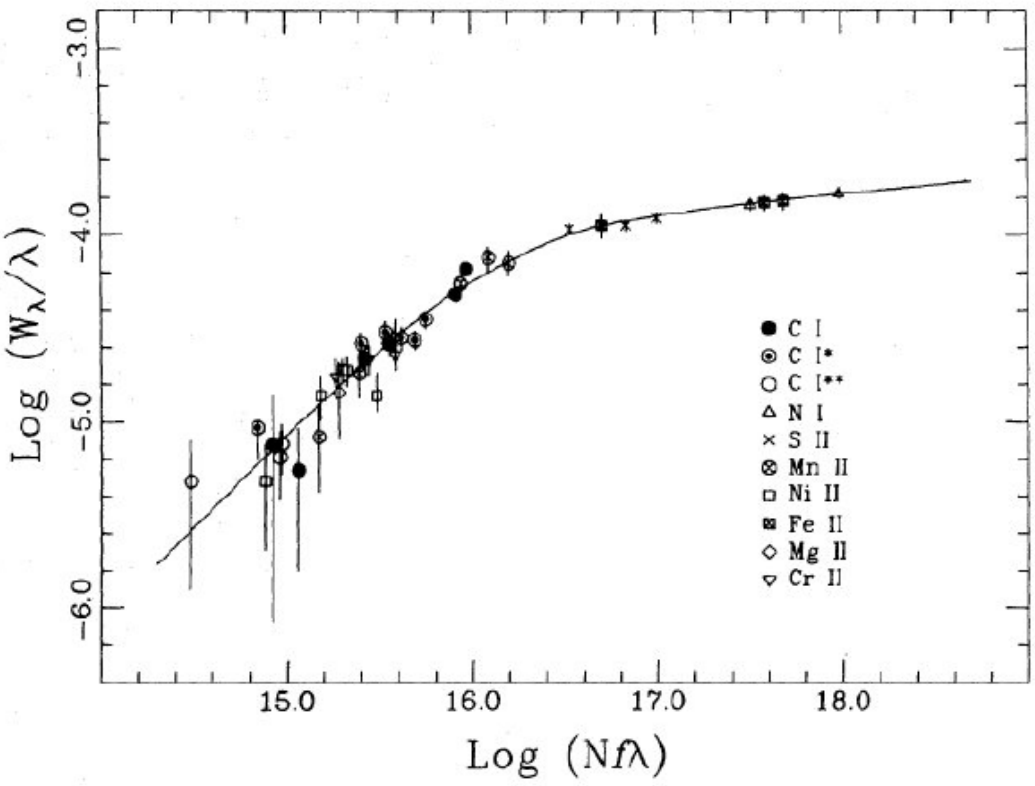

Observational needs for stellar abundance work

- Curve of growth analysis shows that, for weak lines, equivalent widths increase linearly with abundance ⇒ weak lines are preferred for accurate work
- Ideally one requires high resolution (R ~ 50000 – 100000) high S/N spectroscopy
- Most stars are too faint (too distant) to meet these requirements ⇒ go to lower resolution
- Interesting (not complete) abundance information can be obtained at R ~ 500
- Relatively faint (long lived) stars can only be observed individually in our Galaxy
- Studies of stars of different ages can reveal chemical history ⇒ Age – Metallicity relation
- Abundance ratios of different elements provide important clues for chemical evolution
- The brightest giants and supergiants can also be observed in external galaxies up to ~10 Mpc

Chemical analysis: synthetic spectra

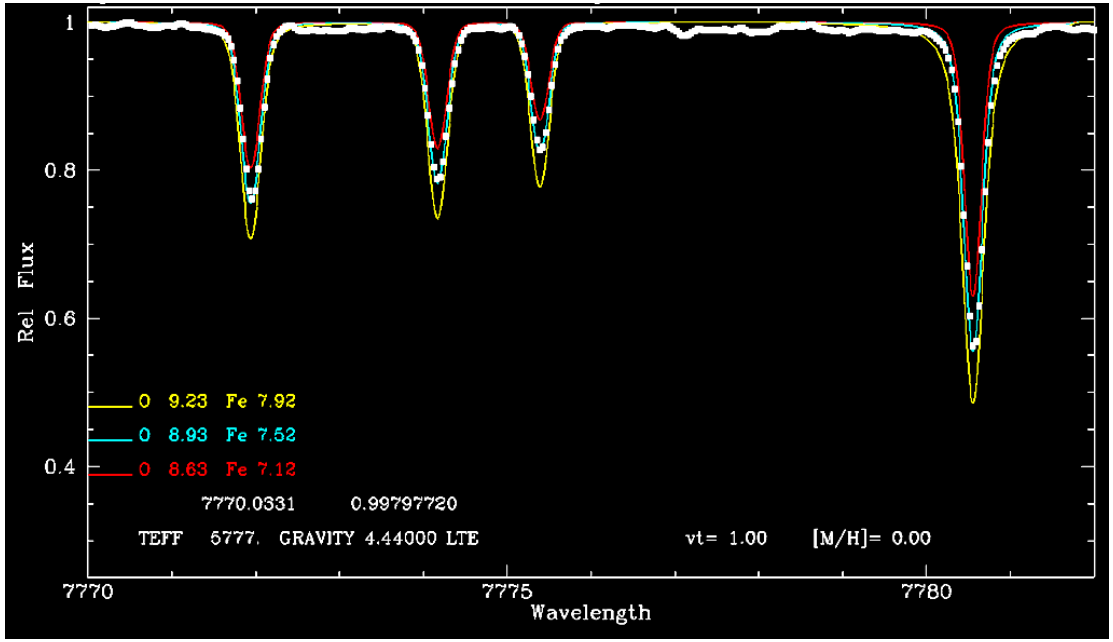

It requires good knowledge of the broadening sources. The best agreement between models and observations is found by minimising residuals: $\chi^2 = \sum(\psi_\lambda - F_\lambda)^2/\Delta\psi_\lambda^2$

Chemical analysis: differential analysis

- Absolute abundances are sensitive to model errors: the different assumptions employed and limits in the knowledge of line formation processes and broadening sources.

$$X_i = 12 + log\frac{N_i}{H}$$

- The use of relative abundances with reference to a star similar to the one observed allows to eliminate systematic errors.
- Many times, relative abundances are calculated with respect to the solar abundances:

$$\left[\frac{X_i}{H}\right] = log\left(\frac{X_i}{H}\right)_* - log\left(\frac{X_i}{H}\right)_{Sol}$$

High resolution stellar spectroscopy

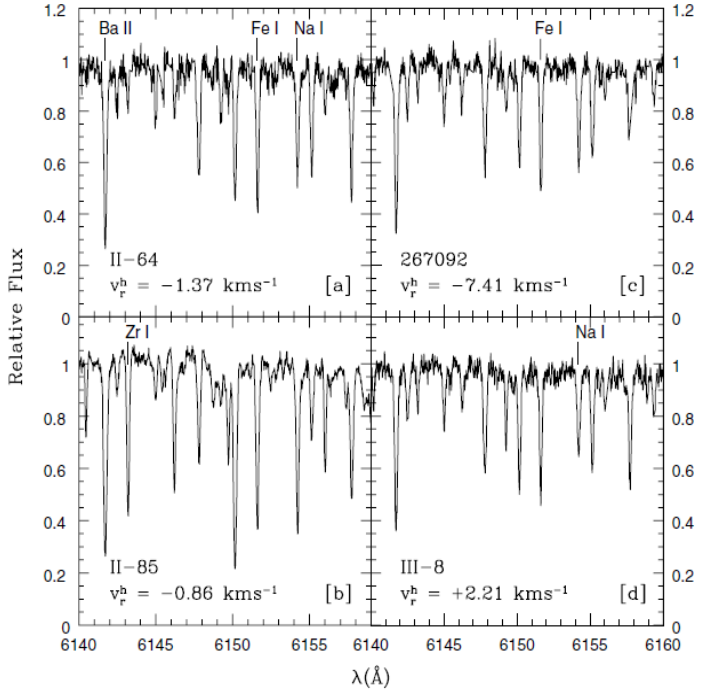

Alves-Brito et al. 2006, A&A, 460, 269

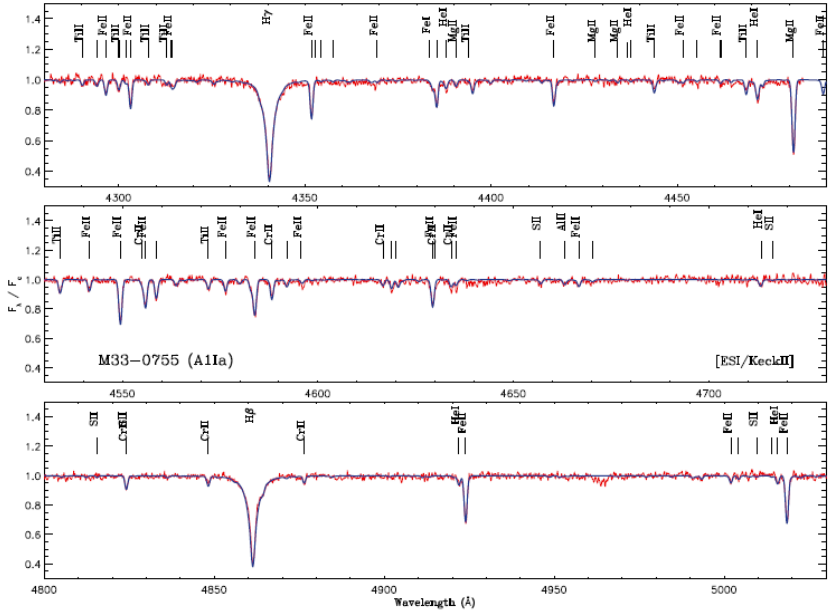

Urbaneja et al. 2007

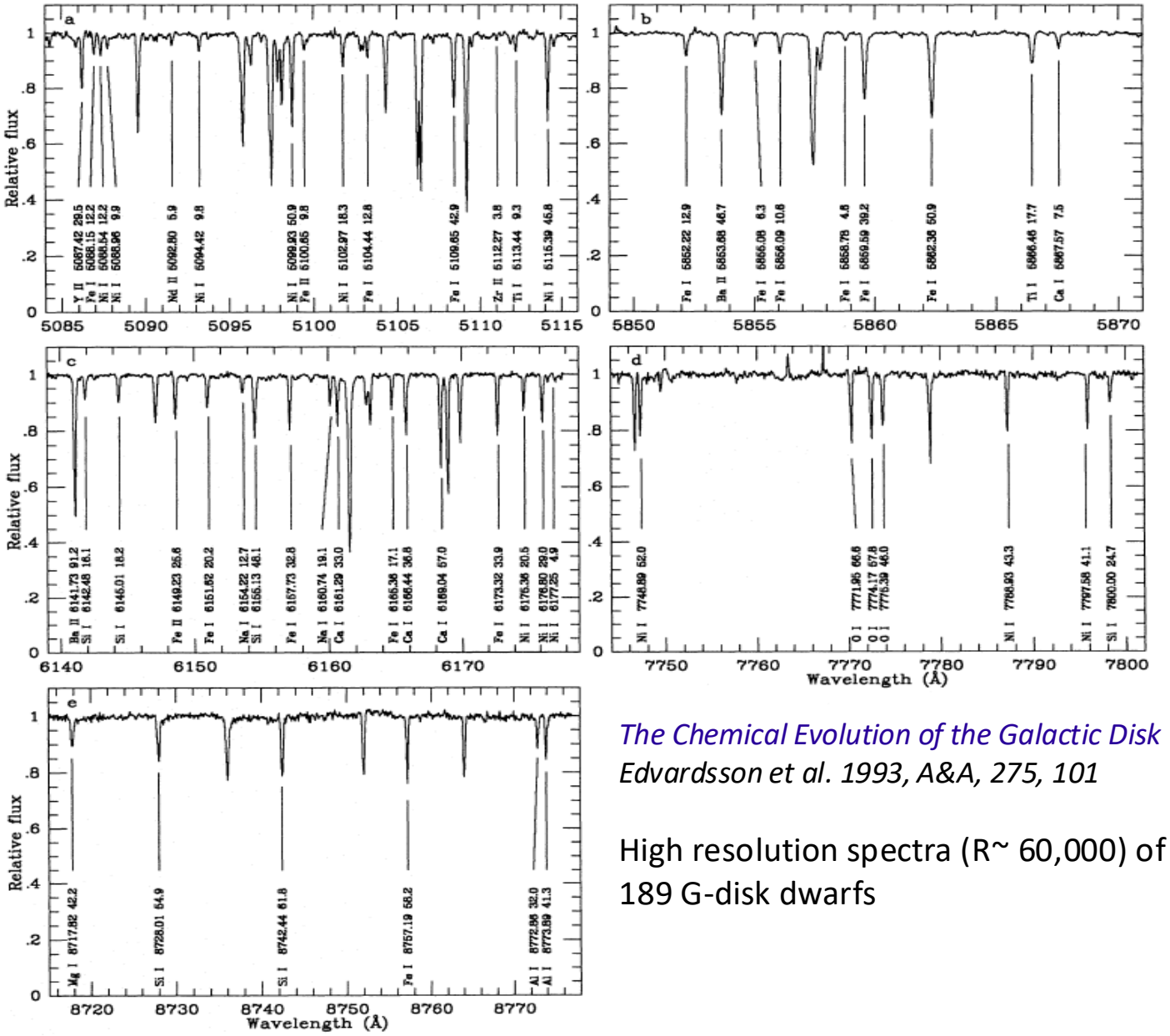

The Chemical Evolution of the Galactic Disk
Edvardsson et al. 1993, A&A, 275, 101

High resolution spectra (R~ 60,000) of 189 G-disk dwarfs

Edvardsson et al. 1993, A&A, 275, 101

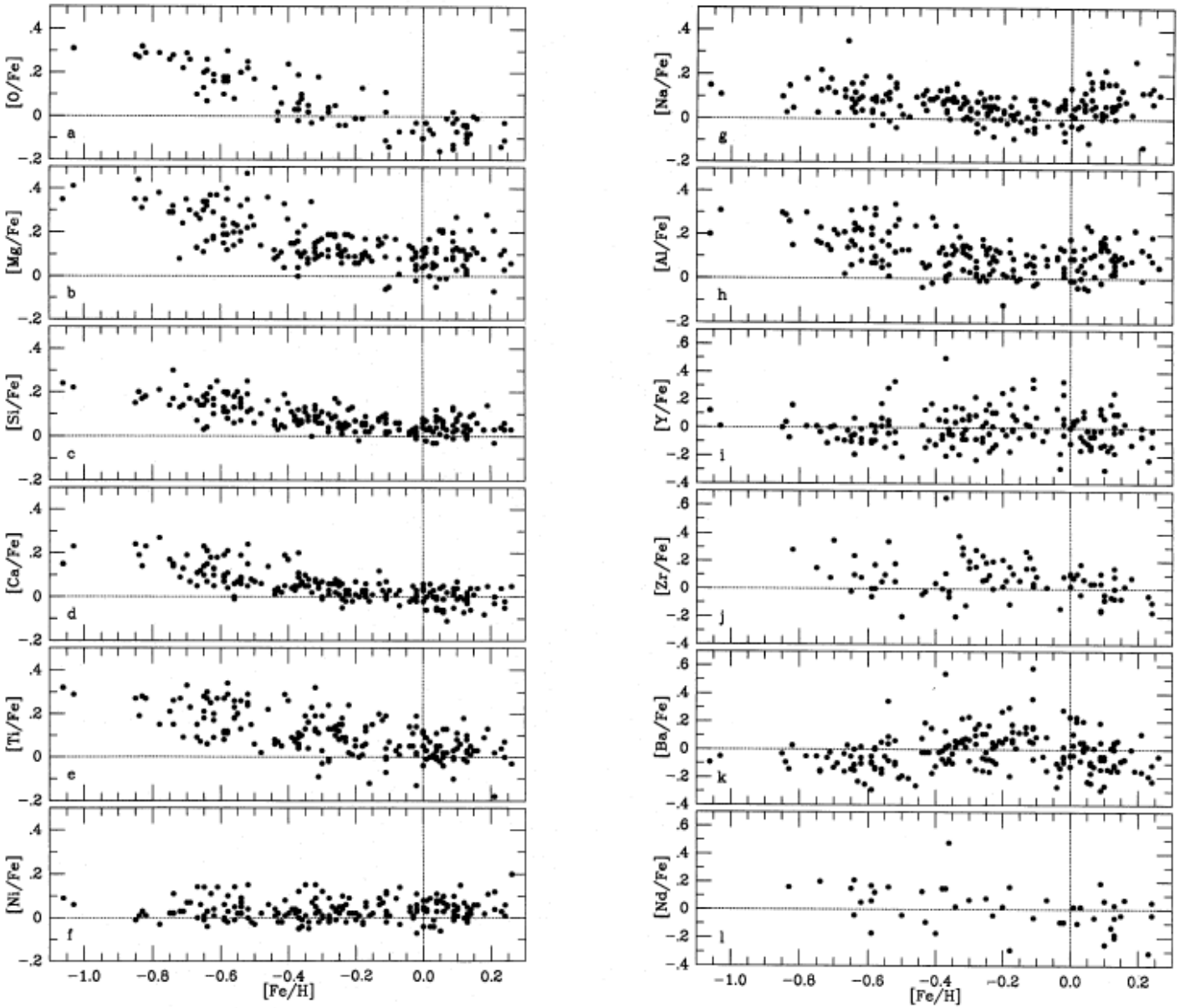

The age-metallicity relation

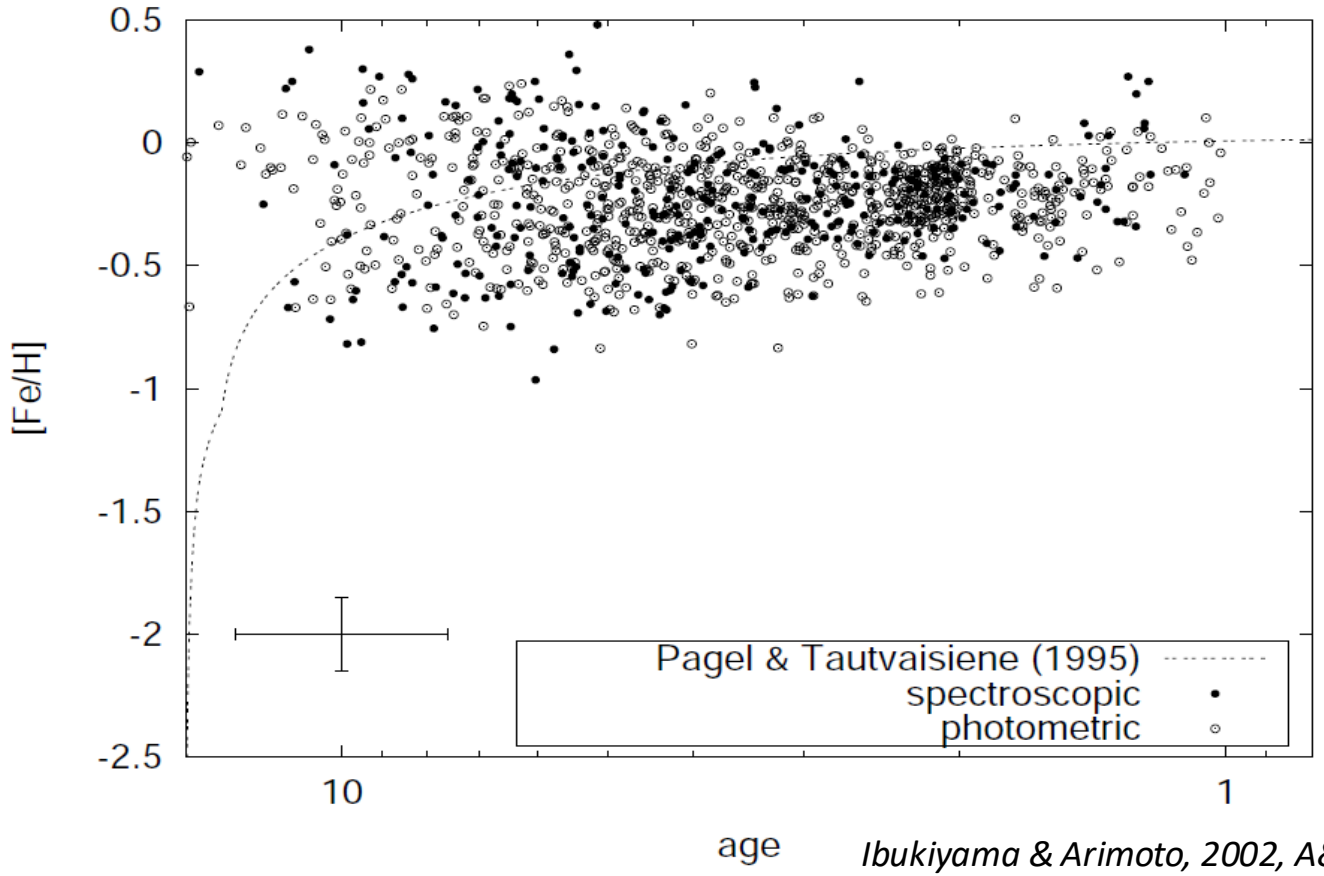

Ibukiyama & Arimoto, 2002, A&A394, 927

Some results for The Galaxy

- The halo has a mean abundance of [Fe/H] ≈ -1.6. Lighter elements are enhanced over Fe with respect to solar. There is no significant abundance gradient.
- The Galactic bulge must have formed very rapidly (≤1 Gyr): its chemical enrichment is dominated by massive stars; it is chemically different from the (local) thin and thick disk; there is a clear radial gradient in [Fe/H] outside 600 pc (Baade's Window), but apparently no gradient inside this radius.

The age-metallicity relation from observations of subgiant stars

Data from Gaia eDR3 + LAMOST DR7 (250,000 subgiant stars)

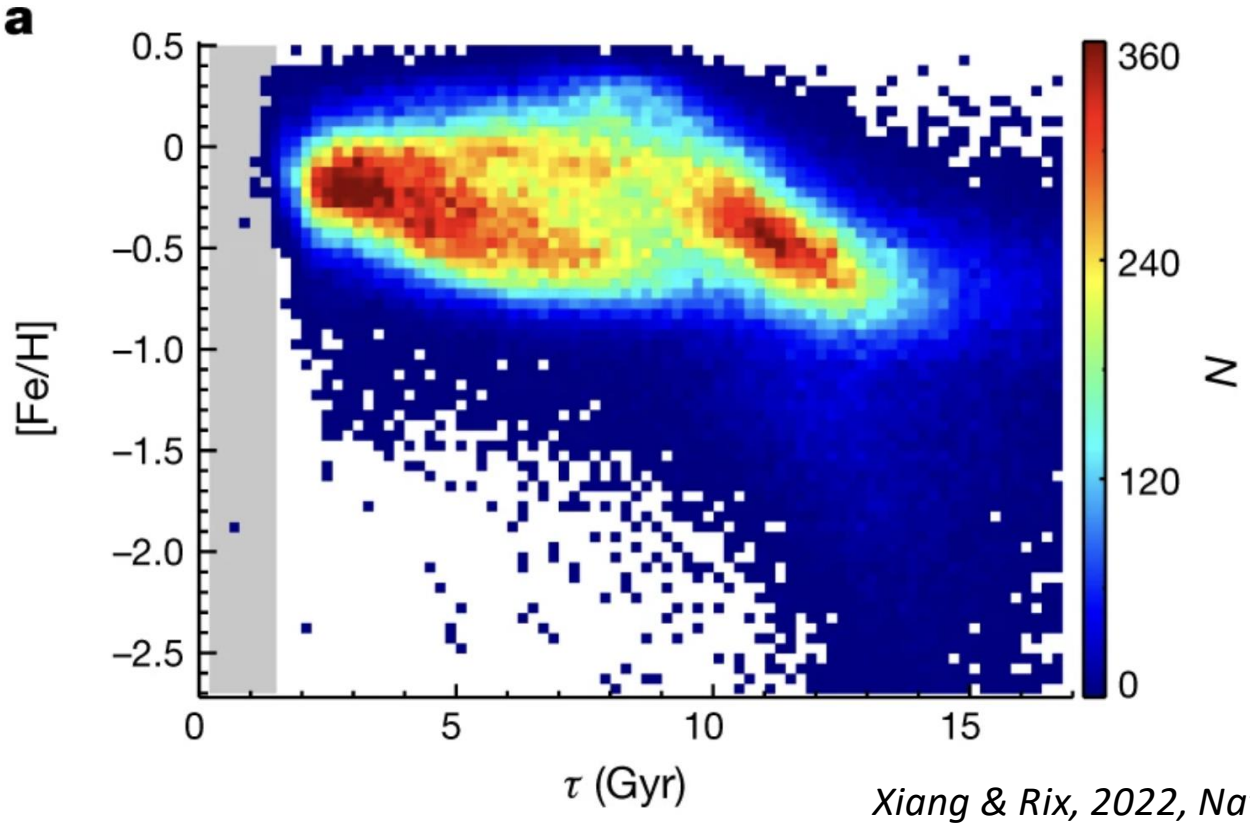

Xiang & Rix, 2022, Nature, 603, 599

Some results for The Galaxy

- It is found that the stellar age–metallicity distribution $p(\tau, [Fe/H])$ splits into two almost disjoint parts, separated at age $\tau \simeq 8$ Ga. The younger part reflects a late phase of dynamically quiescent Galactic disc formation with manifest evidence for stellar radial orbit migration[4,5,6]; the other part reflects the earlier phase, when the stellar halo[7] and the old α-process-enhanced (thick) disk[8,9] formed. These results indicate that the formation of the Galaxy's old (thick) disc started approximately 13 Ga ago, only 0.8 Ga after the Big Bang, and 2 Ga earlier than the final assembly of the inner Galactic halo.

Xiang & Rix, 2022, Nature, 603, 599

Stellar abundance lower limits

- The lowest stellar metallicity has been found for SMSS J031300.36-670839.3, a sub-giant halo star, with an abundance upper limit of -6.5 ⩽ [Fe/H] ⩽ -7.1 (*Keller et al. 2022: Nature 506, 463; Bessel et al. 2015, ApJL,, 806, L16; Nordlander et al. 2017, A&A, 597, 6*) and large over-abundances of C and Mg relative to Ca.
- It is suggested that the star formed from the iron-poor ejecta of a single massive star Population III low energy supernova (SN) which yield large quantities of light elements such as C, but very Little Fe.
- These low energy SN might have been rather common in the early universe.

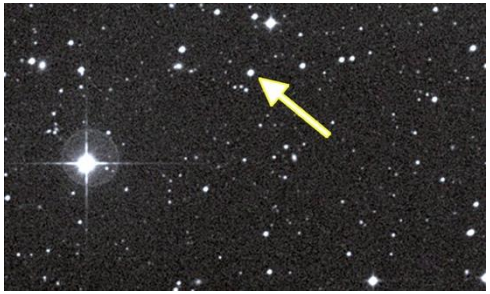

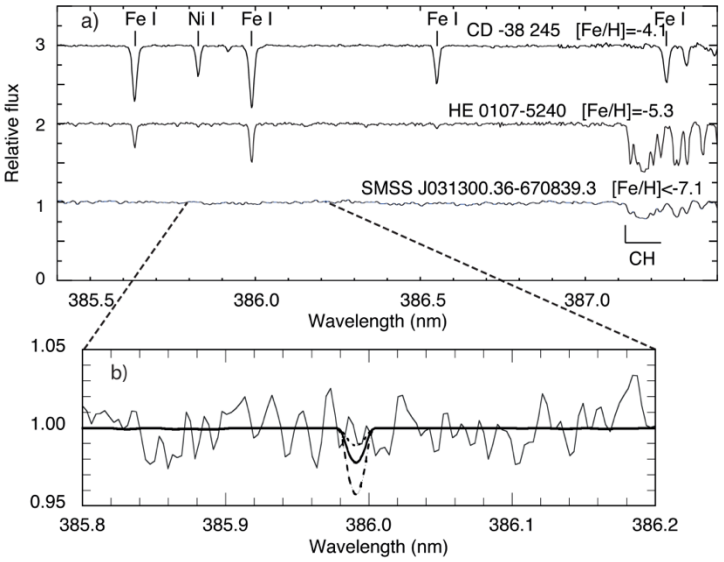

The metallicity distribution function of halo stars

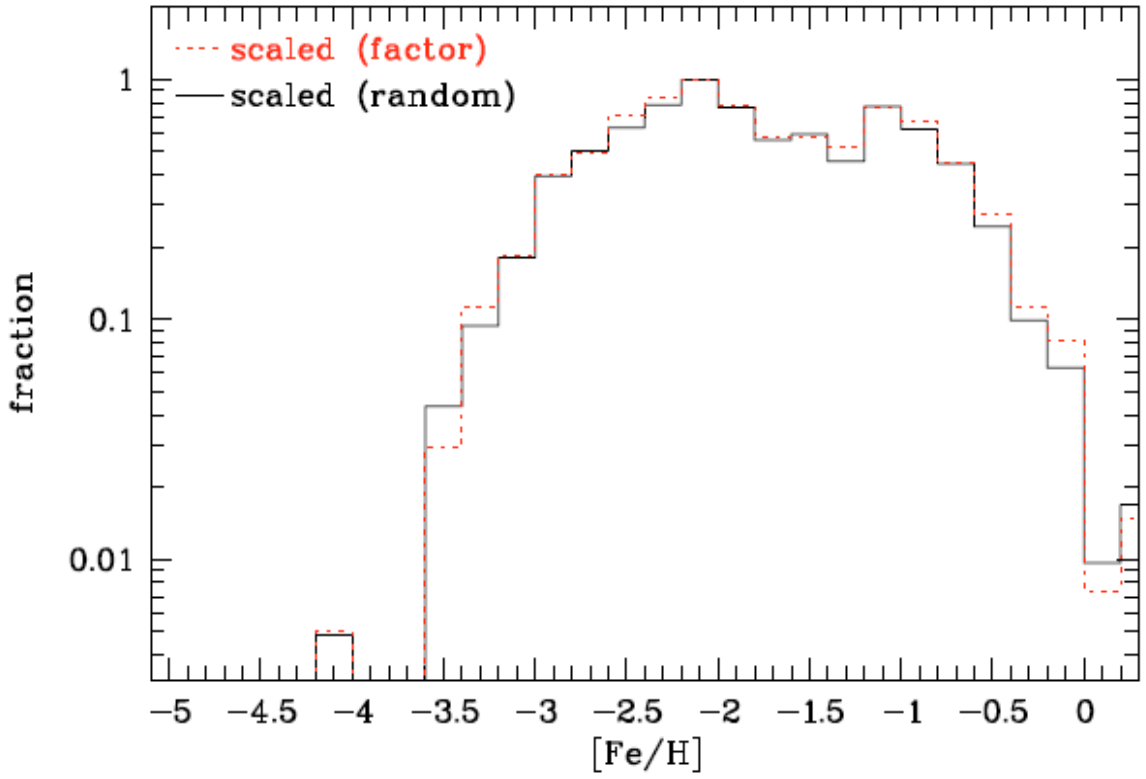

Schörck et al. 2009, A&A, 507, 817

Some results for The Galaxy

- Thick disc: metal abundances overlap with those of the halo (lower end) and the thin disc (high end). No vertical gradient in [Fe/H] is found.

- Thin disc: results come from stars in open clusters and B main sequence stars. Accurate abundances must come from NLTE models. Results should agree with nebular work.

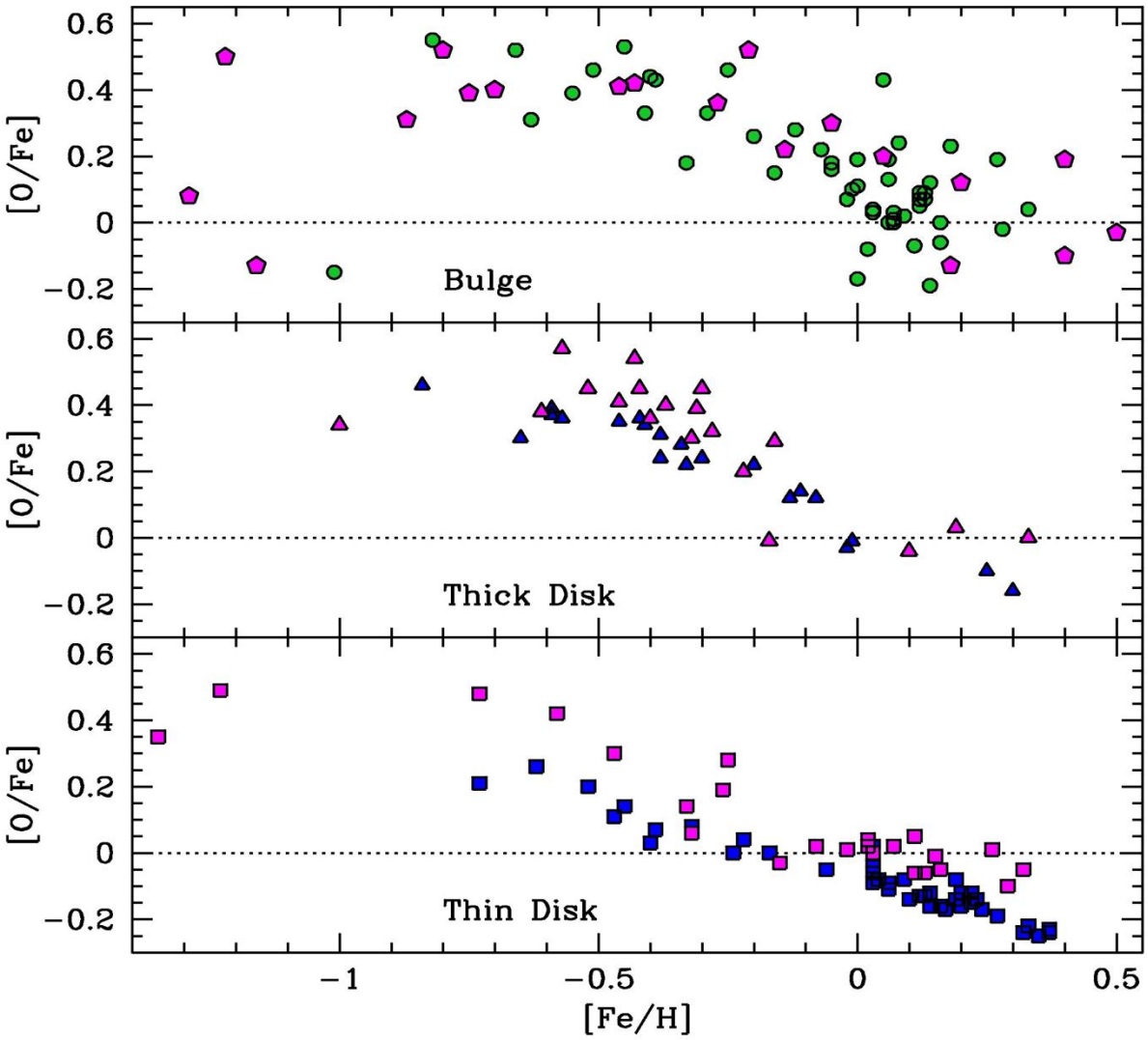

Zoccali et al. 2008, A&A, 486, 177

GAIA- Contribution

Recio-Blanco et al. 2023, *A&A 674, A29 :*
Gaia Data Release 3 Analysis of RVS spectra using the General Stellar Parametriser from spectroscopy

https://www.youtube.com/watch?v=0UkV8OAWE9k

Abundances from integrated spectra

- Apart from the case of galaxies in the Local Group, stars in galaxies appear unresolved and abundances cannot be obtained from stellar spectroscopy.
- Some knowledge can be extracted from the analysis of the stellar light integrated along the line of sight.
- Models of stellar populations in which the integrated galaxy spectra is fitted are used.

Abundances from integrated spectra

- Simple stellar populations, (SSP: single age, single metallicity) are used in combination. Their spectral energy distributions (SEDs) are calculated using stellar evolutionary isochrones that provide information on age and metallicity and theoretical and/or observed individual stellar spectra.
- The existing degeneracy between age and metallicity for a stellar population (both old ages and high metallicities produce, to first order, the same effects in the integrated light) complicates the matter.

Globular star clusters: a Single Stellar Population?

- Frequently stars form in clusters.
- A molecular cloud can contain thousend of dense cores that will evolve to become stars.
- In principle, we can consider that cluster stars :
  - have the same age,
  - are located a the same distance form the observer,
  - are all affected by the same interstellar reddening,
  - have the same metallicity, corresponding to the cloud out of whichthe cluster formed.
- Two different kinds of star clusters are considered, related to the different stellar populations in the Galaxy:
  - **Open** (or galactic) **clusters**→ Population I
  - **Globular clusters**→ Population II

Open clusters

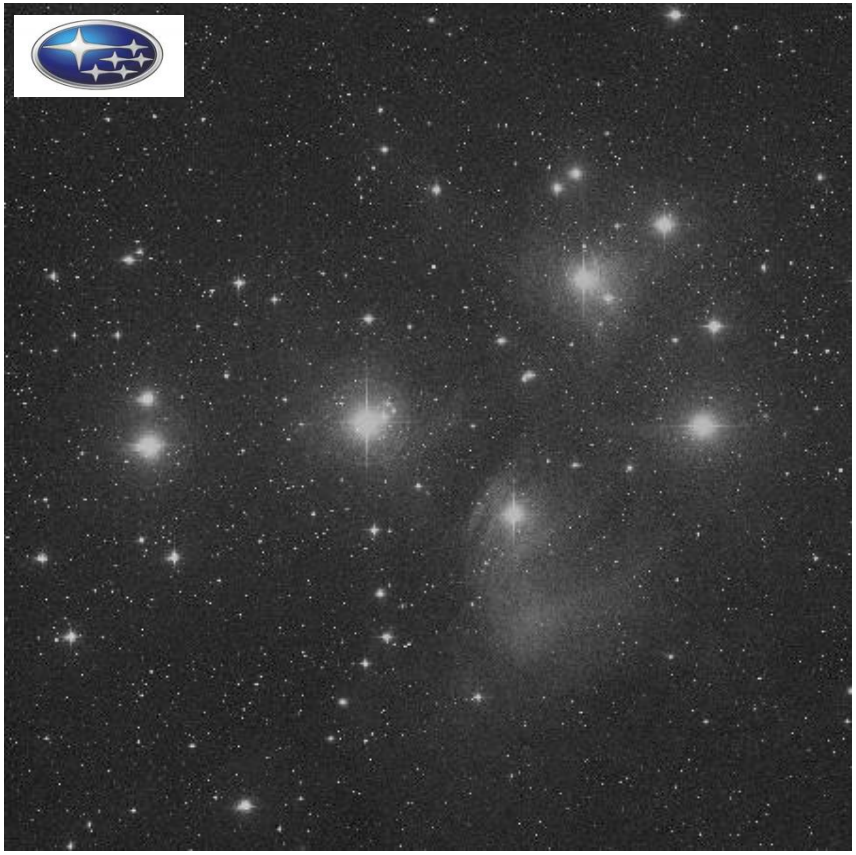

Las Pléyades

NGC 3293

Open cluster characteristics

- **Size**: 1.5 - 20 pc diameter.
- **Star number**: n x 10 – n x 100 .
- **Distance between stars**: ~ 1 pc .
- **Location**: in the Galaxy disc associated to the spiral arms.
- **Number of clusters catalogued in the MWG**: ~ 400
- **Numer of clusters estimated in the Galaxy** ~ 20,000
- **Kinematics**: Moving in almost circular orbits around the galactic centre.

Diagrama Color Magnitud de cúmulos abiertos

- CMD of open clusters showing a Main Sequence (MS) populated by hot and luminous stars and some Red Supergiants (RSG).
- In some cases, some Pre-MS stars are observed.
- Some of them show well developped Giant Branches (GB).

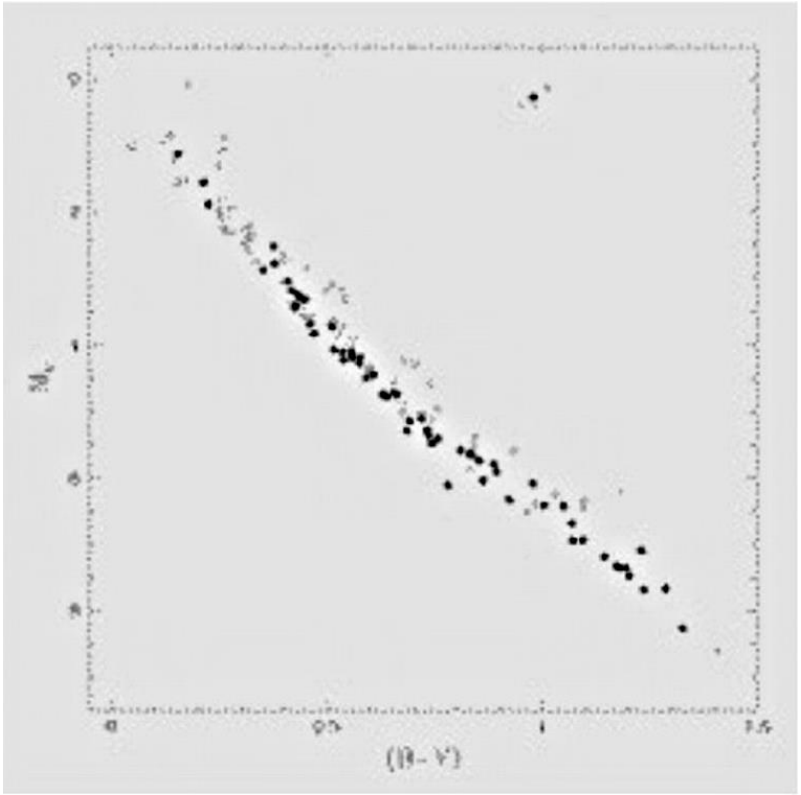

CMD of the Hyades Cluster

Colour-Magnitude Diagrams of open clusters

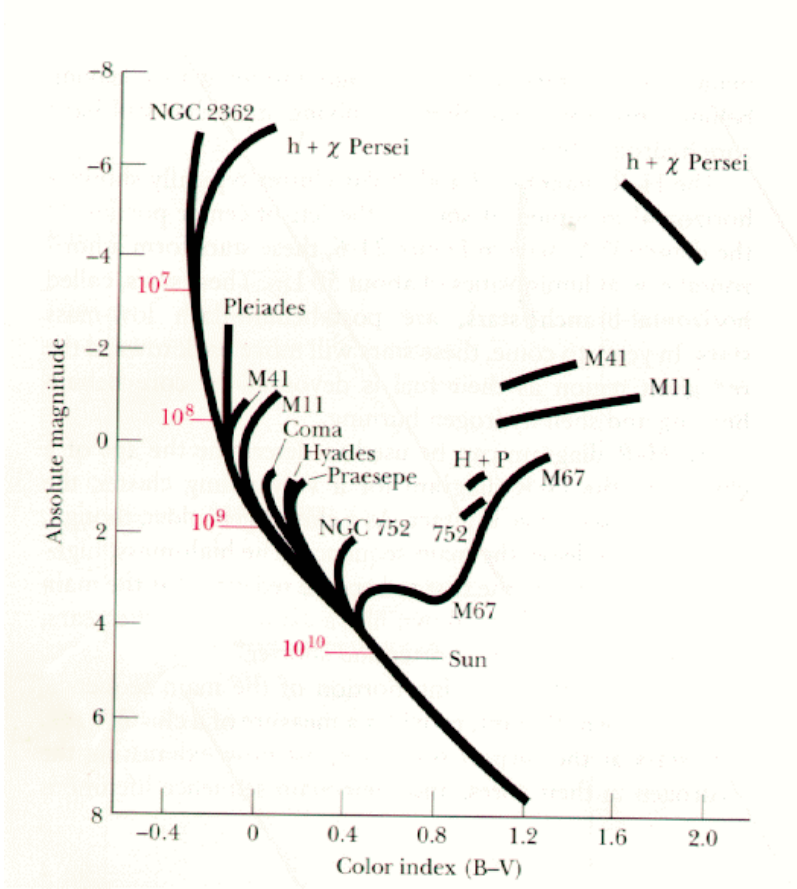

Globular clusters

M3

Omega Cen

Características de los cúmulos globulares

- **Size:** ~ 40 pc diameter.
- **Star number**: n x 10^5 .
- **Distance between stars** : ~ 0.1 pc .
- **Location**: in the Galaxy halo.
- **Number of clusters catalogued in the Galaxy**: ~ 150 .
- **Kinematics** : Moving around the galactic centre in elongated eliptical orbits passing through the Galaxy disc every 10^8 a aproximately.

Colour-Magnitude Diagram of Globular Clusters

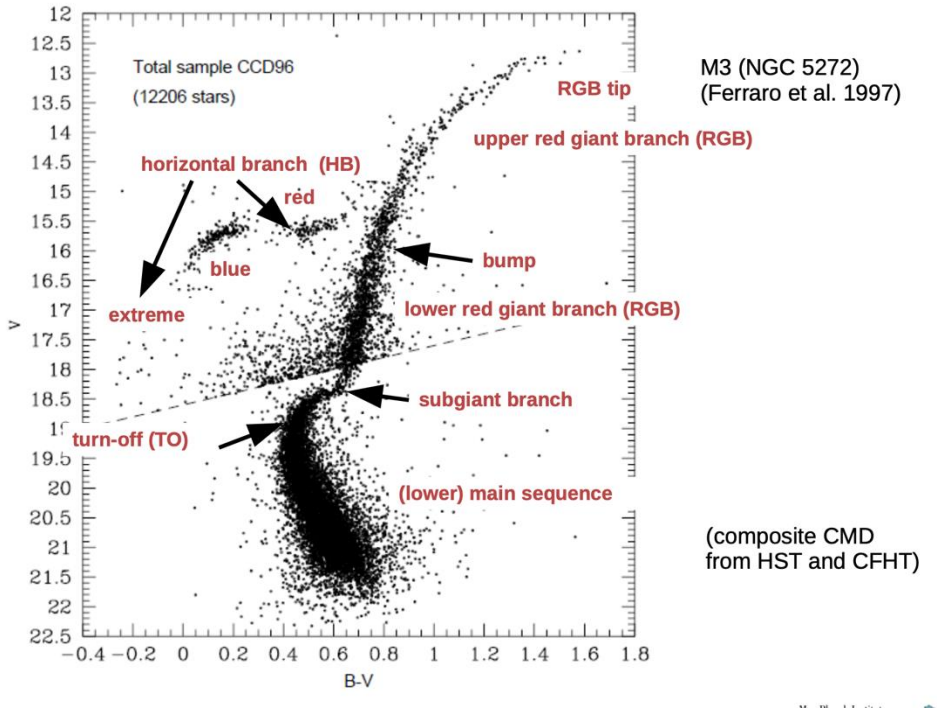

M3 (NGC 5272)
(Ferraro et al. 1997)

(composite CMD
from HST and CFHT)

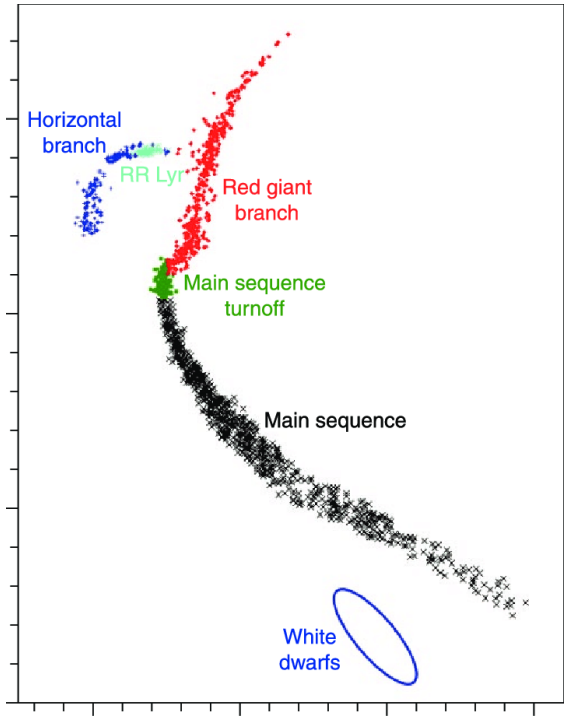

Model fitting: age determination

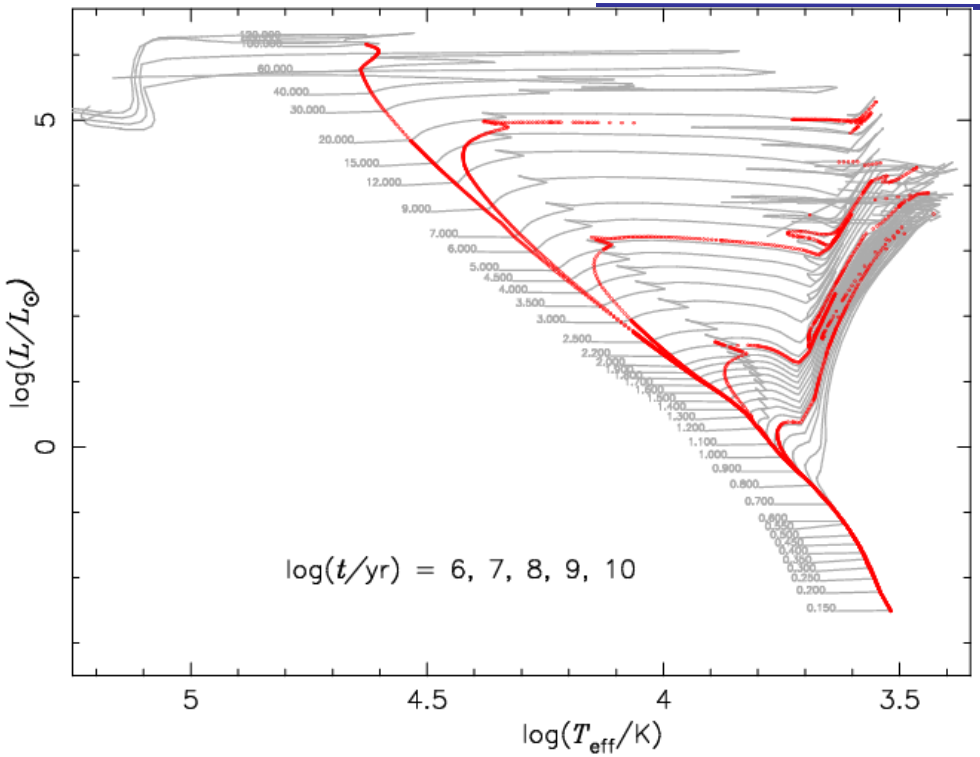

Evolutionary tracks for stars of solar metallicity (grey lines) and isochrones (red lines) corresponding to stars with the same age. Stellar masses are between 0.15 y120 $M_{\odot}$ and isochrone ages are: log(t/a)= 6, 7, 8, 9 and 10.

The importance of deriving accurate globular cluster metallicities

- Globular clusters ages provide unique constraints on cosmology and early epochs of galaxy formation.
- Globular clusters ages cannot be determined without the precise knowledge of their chemical composition
- An error of 0.3 dex in the overall heavy element abundance of a cluster ([Fe/H]) translates into an error of about 3 Gyr in the age derived from fitting an isochrone to accurately derived photometric main-sequence.

The metal abundance of Globular Clusters

- The metallicity of Globular Clusters is determined mainly from spectroscopic observations of of their brighest stars, usually red giant o or red supergiant stars.

- The globular cluster metallicity is usually written as:

$$[Fe/H] = \log (Fe/H) - \log (Fe/H)_{\odot}$$

Photometry: colour of the Giant Branch

Da Costa and Armandroff, 1990

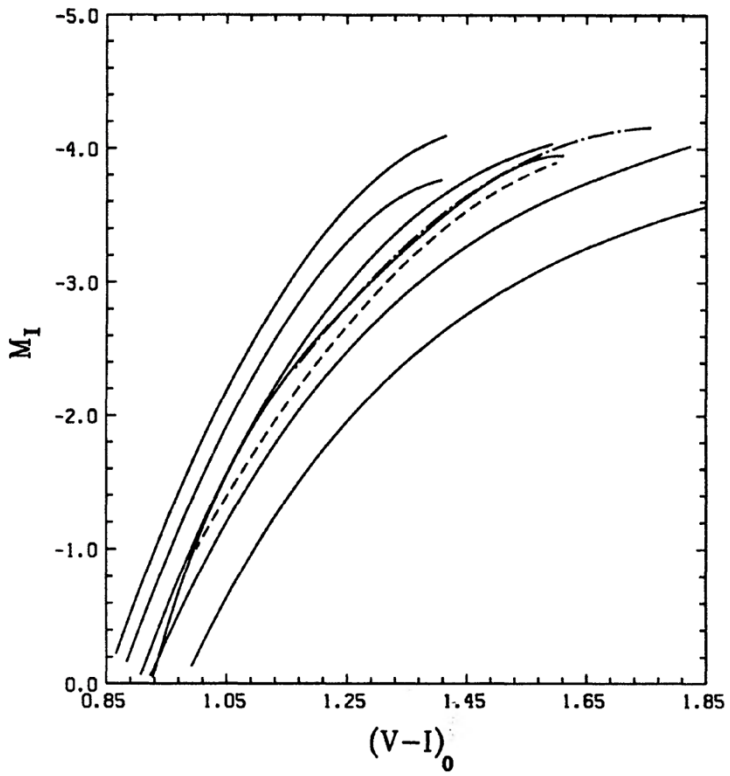

- Giant branch loci in the M_I,$(V-I)_0$ plane of six standard clusters of different (solid curves) together with the giant branches of M5 (dotted-dashed curve) and NGC 362 (dashed curve).
- Metallicity increases to the right.

$$[\mathrm{Fe/H}] = -15.16 + 17.0(V-I)_{0,-3} - 4.9[(V-I)_{0,-3}]^2,$$

Spectroscopy of bright individual stars: the globular cluster Metallicity scale

- Medium-to-high resolution spectroscopy present problems with continuum placement (*see Cohen, 1978: ApJ 223, 487 and Pilachowski et al. 1980: ApJ 236, 508*).
- The use of the CaII Triplet lines in the red part of the spectrum came to solve this problem (*see, for example, Armandroff and Da Costa,1991: AJ 101, 1329*).
- Rutledge et al. 1997 (*PASP 109, 883*) obtained CCD spectra with ~ 4 Å resolution in the region 7250-9000 Å for 976 stars lying near the red-giant branches in color-magnitude diagrams of 52 Galactic globular clusters. Measurements of the equivalent widths of the infrared calcium triplet lines yielded a relative metal-abundance ranking with the necessary precisión.

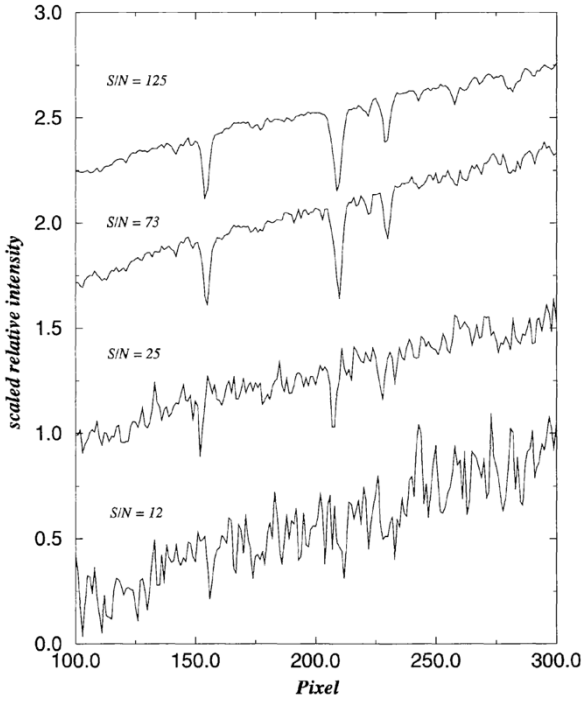

Integrated spectroscopy

- Integrated high resolution spectra can also be used to derive globular cluster metallicities.
- It requires also the use of well sampled CMD of the clusters and theoretical isochrones in combination with standard stellar atmosphere and spectral synthesis codes.
- Examples of this procedure can be found in *Larsen et al. 2017: A&A, 601, 96*.
- This method can also be used for globular clusters in external galaxies (*Larsen et al 2018: A&A, 613, 56*).

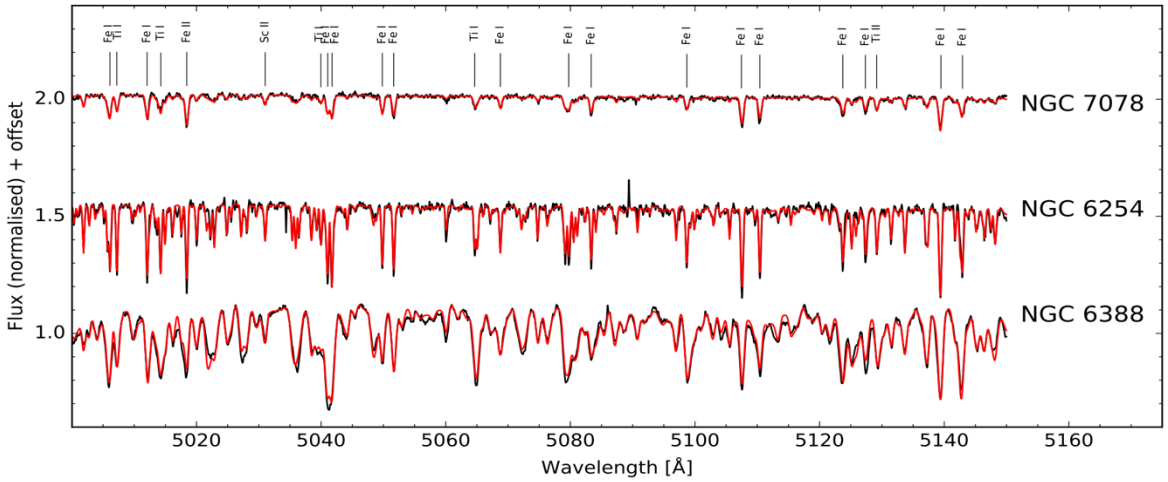

Observed (black lines) and best-fitting model spectra (red lines) for three GCs spanning the full range of metallicities.

Distribution of the metallicity of globular clusters in the Galaxy

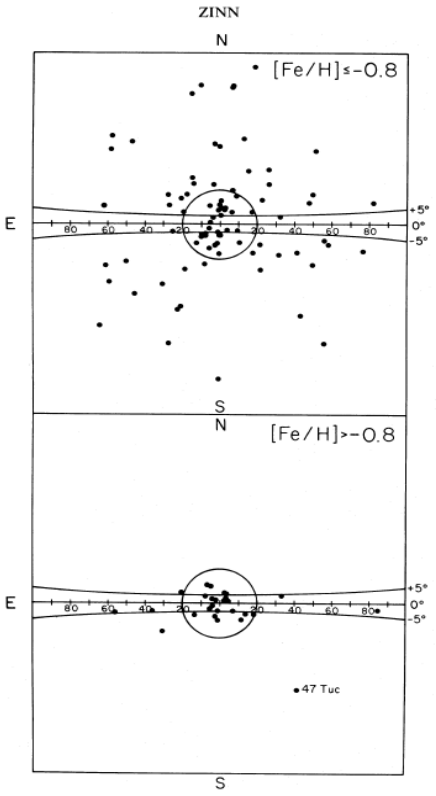

Zinn, R. 1985, ApJ, 293, 424

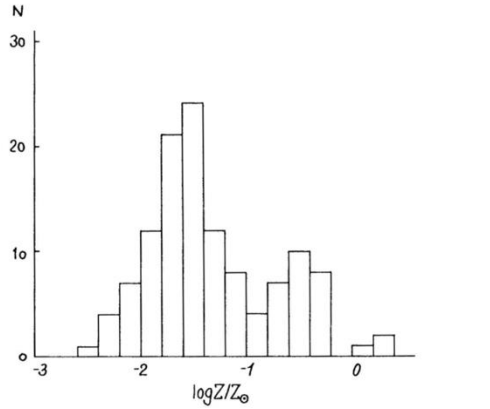

Figure 1. Metallicity histogram of. globular clusters according to Zinn (1985). The two metallicity peaks correspond to two subsets of clusters having very different spatial and kinematical properties.

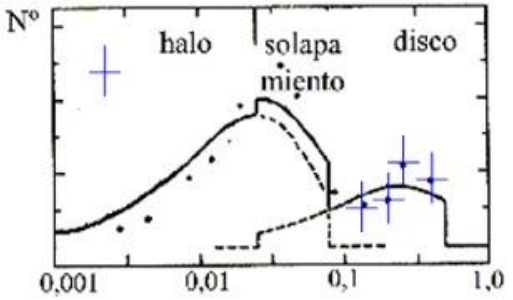

Metalicidad media con respecto al valor solar

Globular Star Clusters: a Single Stellar Population?

- Three observational facts question the paradigm of the assumption of GCs as simple stellar populations.
  - Chemical anomalies in the chemical composition of stars in GCs which is not homogeneous in the elements involved in hot bottom burning, such as C, N, O, Na, Al, and in some cases Mg, Si, and K. Stars with lower N and Na and higher C and O resemble Galactic-field stars with the same metallicity, while stars enhanced in N and Na and depleted in C and O are mostly found in GCs.
  - The so called "second parameter" of the Horizontal Branch (HB), mainly that GCs with similar average metallicities show different (HB) morphologies.
  - The growing evidence of split Main Sequences (MS), Red Giant ranches (RGBs), and Sub-Giant Branches (SGBs) in the CMD of GCs.
- These findings point to the fact that CMDs of nearly all GCs are composed of multiple sequences that can be followed continuously implying the presence of multiple stellar populations.
- A new paradigm is arising for the formation of massive star clusters, which includes several episodes of star formation.

Multiple stellar populations in Globular Star Clusters

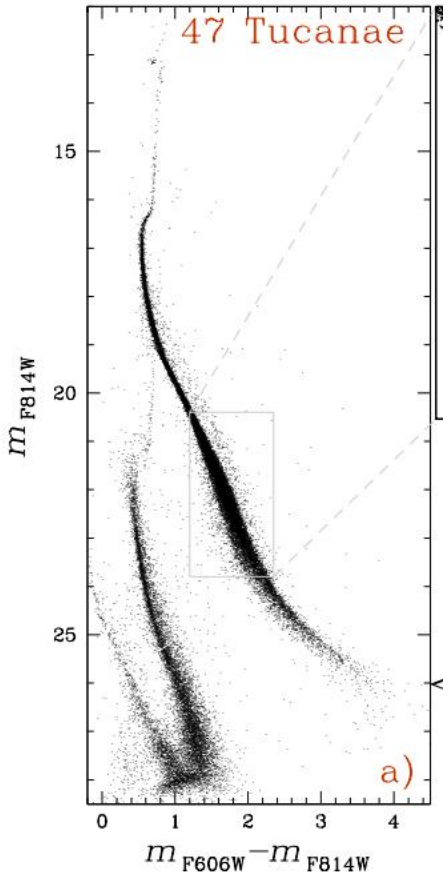

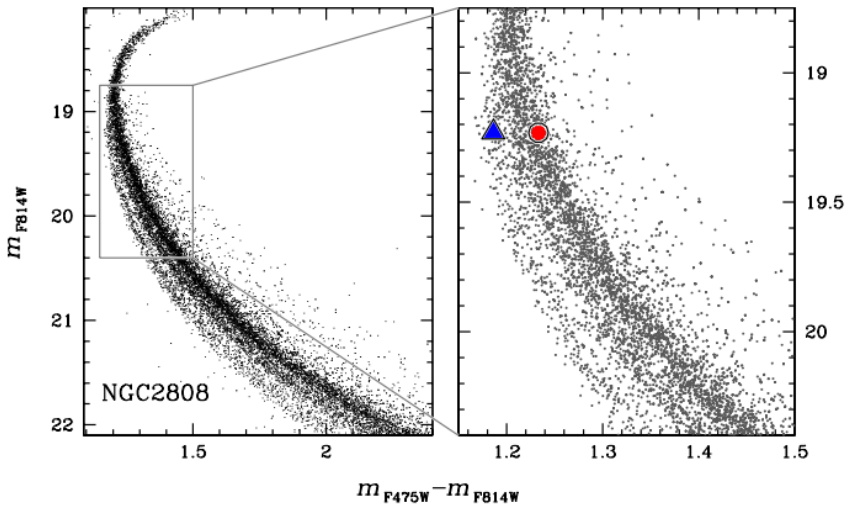

Fig. 1 The triple MS of NGC 2808 (Piotto et al. 2007) and the position of the two MS stars, one on the bMS, one on the rMS, analysed by Bragaglia et al. (2010b).

(See reviews in Gratton, Carretta and Bragaglia, 2012 (2012A&ARv..20...50) and Miloni and Marino, 2022 (Universe, 8, 359)